

AD-A168 433

THREE-DIMENSIONAL STRESS SINGULARITIES IN ANISOTROPIC  
MATERIALS AND COMPOSITES(U) ILLINOIS UNIV AT CHICAGO  
CIRCLE N SOMARATNA ET AL. AUG 85 AMMRC-TR-85-24

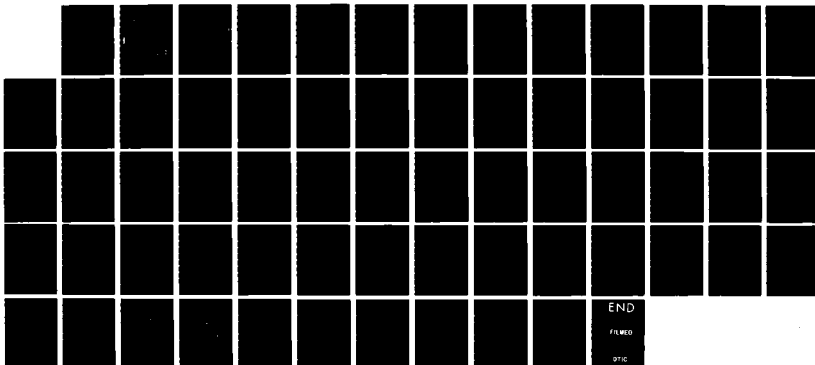
UNCLASSIFIED

DARAG46-83-K-0159

1/1

F/G 12/1

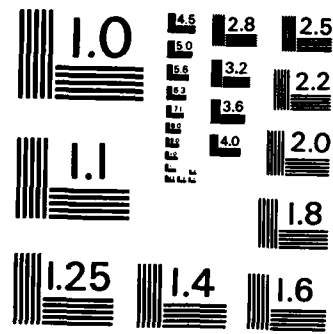
NL



END

FILED

STIC



MICROCOPY RESOLUTION TEST CHART  
NATIONAL BUREAU OF STANDARDS - 1963 - A

(2)

AD-A160 433



AD

AMMRC TR 85-24

THREE-DIMENSIONAL STRESS SINGULARITIES IN  
ANISOTROPIC MATERIALS AND COMPOSITES

August 1985

N. SOMARATNA and T. C. T. TING  
University of Illinois at Chicago  
Dept. of Civil Engineering, Mechanics, and  
Metallurgy  
Chicago, Illinois 60680

FINAL REPORT

Contract No. DAAG46-83-K-0159

Approved for public release; distribution unlimited.

DTIC FILE COPY

DTIC  
ELECTED  
OCT 18 1985  
S D  
B

Prepared for

ARMY MATERIALS AND MECHANICS RESEARCH CENTER  
Watertown, Massachusetts 02172-0001

85 10 18 035

The findings in this report are not to be construed as an official Department of the Army position, unless so designated by other authorized documents.

Mention of any trade names or manufacturers in this report shall not be construed as advertising nor as an official endorsement or approval of such products or companies by the United States Government.

**DISPOSITION INSTRUCTIONS**

Destroy this report when it is no longer needed.  
Do not return it to the originator.

## UNCLASSIFIED

SECURITY CLASSIFICATION OF THIS PAGE (When Data Entered)

REPORT DOCUMENTATION PAGE		READ INSTRUCTIONS BEFORE COMPLETING FORM
1. REPORT NUMBER AMMRC TR 85-24	2. GOVT ACCESSION NO. AD-A160433	3. RECIPIENT'S CATALOG NUMBER
4. TITLE (and Subtitle) THREE-DIMENSIONAL STRESS SINGULARITIES IN ANISOTROPIC MATERIALS AND COMPOSITES	5. TYPE OF REPORT & PERIOD COVERED Final Report 15 Mar 83 - 15 Aug 84	
	6. PERFORMING ORG. REPORT NUMBER	
7. AUTHOR(s) N. Somaratna and T. C. T. Ting	8. CONTRACT OR GRANT NUMBER(s) DAAG46-83-K-0159	
9. PERFORMING ORGANIZATION NAME AND ADDRESS University of Illinois at Chicago Dept. of Civil Engineering, Mechanics, and Metallurgy Chicago, Illinois 60680	10. PROGRAM ELEMENT, PROJECT, TASK AREA & WORK UNIT NUMBERS D/A Project: 8H363304D215 AMCMS Code: 693000.21506	
11. CONTROLLING OFFICE NAME AND ADDRESS Army Materials and Mechanics Research Center ATTN: AMXMR-K Watertown, Massachusetts 02172-0001	12. REPORT DATE August 1985	
14. MONITORING AGENCY NAME & ADDRESS (if different from Controlling Office)	13. NUMBER OF PAGES 61	
	15. SECURITY CLASS. (of this report) Unclassified	
	15a. DECLASSIFICATION/DOWNGRADING SCHEDULE	
16. DISTRIBUTION STATEMENT (of this Report)  Approved for public release; distribution unlimited.		
17. DISTRIBUTION STATEMENT (of the abstract entered in Block 20, if different from Report)		
18. SUPPLEMENTARY NOTES  21		
19. KEY WORDS (Continue on reverse side if necessary and identify by block number) Elasticity; Eigen functions; Three-dimensional . Stress intensity; Anisotropy; ↗ Eigenvalues; Composite materials ↗		
20. ABSTRACT (Continue on reverse side if necessary and identify by block number)		
(SEE REVERSE SIDE)		

**UNCLASSIFIED**

**SECURITY CLASSIFICATION OF THIS PAGE (When Data Entered)**

**Block No. 20**

5-20-1

**ABSTRACT**

→ A general numerical procedure is presented for determining the 3-dimensional stress singularities in anisotropic materials and composites. The geometry near the singular point can be represented by a conical wedge whose lateral surface is generated by straight lines passing through the wedge apex. The shape  $S_1$  of the cross section of the conical wedge at any constant radial distance defines the geometry of the 3-dimensional singular point in the material. If  $S_1$  consists of two regions each occupied by a different material, we have a 3-dimensional composite conical wedge. A finite element scheme based on variational principles is used to find the order of stress singularities at the wedge apex. The method can be applied to any shape of  $S_1$ . Several examples are presented. For comparisons with the existing numerical schemes for isotropic materials, the method is applied to special geometry and to isotropic materials. It is shown that the 8 node higher order isoparametric elements employed here is very efficient in obtaining a fairly accurate result. Keyw...  
1

**UNCLASSIFIED**

**SECURITY CLASSIFICATION OF THIS PAGE (When Data Entered)**

#### ACKNOWLEDGEMENTS

This work is supported by the Army Materials and Mechanics Research Center (AMMRC), Watertown, Massachusetts under Contract No. DAAG 46-83-K-0159 with the University of Illinois at Chicago, Chicago, Illinois. Mr. J. F. Dignam of the AMMRC was the project manager and Dr. S. C. Chou was the technical monitor. The support and encouragements of Mr. Dignam and Dr. Chou are gratefully acknowledged. The authors are also grateful to Professor Z. P. Bazant and Dr. L. F. Estenssoro for valuable discussions during the course of this research.



Accession For	
NTIS	DTIC
DTIC Title	<input checked="" type="checkbox"/>
Uncontrolled	<input type="checkbox"/>
Justification	
By _____	
Distribution/	
Availability Codes	
Dist	Avail Ind/or Special
A-1	

## TABLE OF CONTENTS

	<u>Page</u>
ABSTRACT	
ACKNOWLEDGEMENTS	
1. Introduction .....	1
2. Formulation	
2.1 Variational Principle .....	5
2.2 Descretized Formulation .....	11
2.3 The Element .....	15
2.4 Evaluation of .....	17
3. Test Problems	
3.1 3-D Crack in Isotropic Materials .....	18
3.2 Axisymmetric Notch in Transversely Isotropic Material..	20
4. An Application to Composite Materials .....	23
5. Stress Singularities at Other Three-Dimensional Corners	
5.1 Exterior Problem .....	28
5.2 Interior Problem .....	29
6. Concluding Remarks .....	31
REFERENCES .....	33
APPENDIX A .....	35
TABLES .....	38
FIGURES .....	45

## 1. INTRODUCTION

Since the creation of a light weight composite for the space industry, composite materials have now been widely used in many areas of the industry. Due to the geometrical and material discontinuity in the composite, stress singularities often occur resulting in the failure of the composite. In order to understand the failure mechanism and to help designing a better composite, it is essential to analyse the nature of stress distribution near a singular point in the composite. One of the reasons for the slow progress in designing a more durable composite is the lack of rigorous stress analyses near a stress singularity, especially when the singularity is a three-dimensional one. Even though many investigations have been carried out on the nature of stress singularities in 2-dimensional elasticity problems, only a relatively little work has been done in the area of stress singularities in general 3-D problems. This may be partly due to the complexities of the problem itself. Nevertheless, in practice, both in the areas of fracture mechanics and general stress analysis a knowledge of the 3-D stress singularities would be quite useful. In an excellent review article on the three dimensional stress problem for a cracked plate Sih [1] discusses at length the difficulties associated with the task of obtaining an analytical solution. Most of the time in analytical studies special material properties and geometries that make it possible to reduce the problem to two dimensions in mathematical terms have been employed. An extensive collection of such analysis is presented in [2] and further discussions on 3-D analyses can be found in [3]. More recently Parihar and Keer [4,5] have presented analytical solutions for wedge-shaped cracks, inclusions and stamps in isotropic materials. Such special problems serve as extremely useful 'bench mark' tests

for other more general methods such as the one that would be described herein. However, in the more general case of a three dimensional singularity in a completely anisotropic material, obtaining an analytical solution seems quite difficult except for special cases [6] and numerical methods have to be employed. The present study is aimed at proposing one such numerical method, viz. a finite element scheme.

A general numerical procedure for determining 3-D singularities was first developed by Bazant [7] for harmonic functions and by Bazant and Estenssoro [8,9] for isotropic elastic materials who used it to study the singularities at the intersection of free surface and cracks. Their results for a crack orthogonal to a free surface were in good agreement with the results obtained via a semi-analytical method by Benthem [10,11]. However no solutions are available for anisotropic materials.

The present finite element scheme is an extension of that developed by Bazant and Estenssoro [9] to incorporate general anisotropic elastic materials. In Section 2 we present the general formulation of the finite element scheme. Testing of the method against some known results will be described in Section 3. In Section 4 it is applied to study a problem in laminated composite materials and finally in Section 5 we use it to study the possible occurrence of stress singularities in other 3-D corners.

Let  $(r, \theta, \phi)$  refer to spherical co-ordinates and consider the region near the apex of a conical wedge (a notch or a rigid inclusion) in which the apex is the origin of the co-ordinates, Fig. 1. The lateral surface  $S_2$  of the conical wedge is assumed to be generated by radial lines. The cross section of the conical wedge at any constant radius is denoted by  $S_1$ . The boundary of  $S_1$ ,

which specifies the shape of  $S_2$ , is given by the equation  $\psi(\theta, \phi) = 0$ . Depending on whether a notch or a rigid inclusion is being analysed the homogeneous boundary conditions applicable on  $S_2$  will be either traction free condition or rigidly clamped condition respectively. Since we are interested in the possible stress singularities near the apex, the boundary conditions on  $S_1$  need not be specified.

For the purpose of an asymptotic analysis for possible stress singularities at the apex of the conical region we seek non-trivial displacement solutions of the form

$$\left. \begin{array}{l} u = r^\lambda f(\theta, \phi) \\ v = r^\lambda g(\theta, \phi) \\ w = r^\lambda h(\theta, \phi) \end{array} \right\} \quad (1)$$

where  $(u, v, w)$  are the components of displacement in  $(r, \theta, \phi)$  directions respectively. This displacement field is required to satisfy equations of equilibrium within the conical region and the relevant homogeneous boundary conditions on the lateral surface  $S_2$ .

A value of  $\lambda$  that would satisfy these conditions is called the eigenvalue and the corresponding functions  $f(\theta, \phi)$ ,  $g(\theta, \phi)$  and  $h(\theta, \phi)$  are called the eigenfunctions. There are infinitely many such eigenstates [12]. But in the present case our attention will be confined to those eigenstates that would lead to stress singularities at the apex. When displacements are of the form given by equation (1) the stresses are proportional to  $r^{\lambda-1}$ . Hence a stress singularity occurs at the origin when  $\lambda < 1$ . On the other hand, for the strain energy to be bounded at the origin we require  $\lambda > -\frac{1}{2}$ . However,  $\lambda < 0$  implies that the

displacements are unbounded at  $r = 0$  which is physically unrealistic unless a concentrated load is applied at the wedge apex. Therefore we are primarily interested in eigenvalues  $\lambda$  in the range  $0 < \lambda < 1$ . The most important would be the smallest  $\lambda$  (i.e., closest to 0) which would give rise to the strongest singularity. If  $\lambda$  is complex, we are interested in the case where  $0 < \operatorname{Re}(\lambda) < 1$ . During this procedure no particular boundary conditions are prescribed at the surface  $S$ , of the cone. The tacit assumption is that by superposing a sufficient number of eigenstates they can be satisfied.

In order to evaluate  $\lambda$  (and  $f(\theta, \phi)$ ,  $g(\theta, \phi)$  and  $h(\theta, \phi)$ ) that would satisfy the above conditions, Bazant and Estenssoro [9] developed a finite element scheme based on a variational principle involving those quantities. Even though they considered only isotropic materials, with a few changes in the details their approach can be used for general anisotropic materials. In the next section we shall present the general formulation. In [9] it has been shown that the variational principle does not yield a minimum principle and that the resulting system of equations for the determination of  $\lambda$  is non symmetric. Those proofs are valid for the present formulation also.

## 2. FORMULATION

### 2.1 VARIATIONAL PRINCIPLE

Normally problems of elasticity can be solved by the use of stationary energy principles. In the present case too we can base our solution procedure on them. However, some special considerations and procedures are required due to the fact that the solutions we seek are not expected to satisfy all the boundary conditions of the problem; they need satisfy only the near field boundary conditions.

For the conical solid shown in Fig. 1 the two boundaries are  $r = r_0$  and  $\psi(\theta, \phi) = 0$  and are denoted by  $S_1$  and  $S_2$ , respectively. Our intention is to find a set of eigenfunctions for the displacement field in the form of equation (1) that would satisfy the necessary boundary conditions near the origin - i.e. on  $S_2$ . Nothing is said about the boundary conditions at the far end - i.e. on  $S_1$ . The hope is that by superposing a sufficient number of eigenfunctions, boundary conditions on  $S_1$  may be satisfied. In fact the cone shown in Fig. 1 should be considered only as one part of a boundary value problem and matching the solution for the cone with that for the adjoining region on  $S_1$  is not of immediate concern.

The eigenfunctions we seek are therefore required to satisfy the governing differential equations and only some of the boundary conditions of the complete elasticity problem for the cone. It is due to this reason that some modifications to the stationary energy principles are needed for the present problem. These modifications were first proposed by Bazant and Estenssoro [9]. We too follow their procedure with a slightly different presentation of the rationale behind the modification.

Once again consider the conical region shown in Fig. 1. When it is subjected to some displacement field a certain traction will result on the boundary  $S_1$ .

Let that traction be denoted by  $\underline{p} = (p_r, p_\theta, p_\phi)$ . If one were to solve the complete problem of which this cone is only a part, one would have to match these tractions and displacements on  $S_1$ , with those of the adjoining region. But for the purpose of our local analysis consider instead the cone to be subjected to external traction  $\underline{p}$  on  $S_1$ . Then the cone should be in equilibrium and the displacement field should satisfy the equations of equilibrium inside the cone and the relevant boundary conditions on  $S_1$  and  $S_2$ . For this situation we can write the principle of minimum potential energy as

$$\delta U - \int_{S_1} (p_r \delta u + p_\theta \delta v + p_\phi \delta w) r^2 \sin \theta d\theta d\phi = 0 \quad (2)$$

where

$$U = \int_V \Phi dr d\theta d\phi \quad (3)$$

is the total strain energy in the volume  $V$  of the cone and

$$\Phi = E r^2 \sin \theta \quad (4)$$

where  $E$  is the strain energy density.  $\delta$  indicates the variations due to kinematically admissible variations in the displacement field  $(u, v, w)$ .  $E$  is a function of the strains  $\epsilon_{ij}$  and they in turn are functions of the displacements and their first derivatives. Therefore we get

$$\delta U = \int_V (\Phi_u \delta u + \Phi_{u_r} \delta u_r + \dots + \Phi_{w_\phi} \delta w_\phi) dr d\theta d\phi \quad (5)$$

where the subscripts  $r, \theta, \phi$  denote partial differentiation.  $\Phi_u$  refers to the partial derivative of  $\Phi$  with respect to  $u$ , assuming  $u, u_r, u_\theta, \dots, w_\phi$  to be independent variables and so on.

Equation (2) implies all the equations associated with the problem of elasticity. But the eigenfunctions need not satisfy the far field boundary condi-

tions on  $S_1$ . Therefore we will modify (2) into a form that would allow those boundary conditions to be separated out from the others. Substitute (5) into (2) and integrate the terms containing  $\delta u_r$ ,  $\delta v_r$  and  $\delta w_r$  by parts in the  $r$  direction to yield:

$$\begin{aligned} \delta \bar{U} + \int_{S_1} [\Phi_{u_r} \delta u + \Phi_{v_r} \delta v + \Phi_{w_r} \delta w] d\theta d\phi \\ - \int_{S_1} (p_r \delta u + p_\theta \delta v + p_\phi \delta w) r^2 \sin \theta d\theta d\phi = 0 \end{aligned} \quad (6)$$

where,

$$\begin{aligned} \delta \bar{U} = \int_V \left[ \left\{ \Phi_u - \frac{\partial}{\partial r} (\Phi_{u_r}) \right\} \delta u + \Phi_{u_\theta} \delta u_\theta + \Phi_{u_\phi} \delta u_\phi \right. \\ \left. + \left\{ \Phi_v - \frac{\partial}{\partial r} (\Phi_{v_r}) \right\} \delta v + \Phi_{v_\theta} \delta v_\theta + \Phi_{v_\phi} \delta v_\phi \right. \\ \left. + \left\{ \Phi_w - \frac{\partial}{\partial r} (\Phi_{w_r}) \right\} \delta w + \Phi_{w_\theta} \delta w_\theta + \Phi_{w_\phi} \delta w_\phi \right] dr d\theta d\phi \end{aligned} \quad (7)$$

To evaluate  $\Phi_{u_r}$ ,  $\Phi_{v_r}$  and  $\Phi_{w_r}$  first evaluate  $E_{u_r}$ ,  $E_{v_r}$  and  $E_{w_r}$ . Note that  $\partial E / \partial \epsilon_{ij} = \sigma_{ij}$  where  $\sigma_{ij}$  is the stress. Since  $\epsilon_{ij}$  is related to  $u$ ,  $u_r, \dots$  through the strain - displacement relations in spherical co-ordinates,  $E_{u_r}, \dots$  can be easily evaluated using the chain rule. We then obtain  $\Phi_{u_r}, \dots$  by the use of (4). When these algebraic manipulations are carried out we get

$$\left. \begin{aligned} \Phi_{u_r} &= r^2 \sigma_{rr} \sin \theta \\ \Phi_{v_r} &= r^2 \sigma_{r\theta} \sin \theta \\ \Phi_{w_r} &= r^2 \sigma_{r\phi} \sin \theta \end{aligned} \right\} \quad (8)$$

Substitution of (8) into (6) yields

$$\delta \bar{U} + \int_{S_1} [ (\sigma_{rr} - p_r) \delta u + (\sigma_{r\theta} - p_\theta) \delta v + (\sigma_{r\phi} - p_\phi) \delta w ] r^2 \sin \theta d\theta d\phi = 0 \quad (9)$$

which implies

$$\delta \bar{U} = 0, \quad (10)$$

$$\left. \begin{array}{l} \sigma_{rr} = p_r \\ \sigma_{r\theta} = p_\theta \\ \sigma_{r\phi} = p_\phi \end{array} \right\} \text{on } S_1 \quad (11)$$

Equation (11) is in fact the traction boundary condition on  $S_1$ . Since we started with a variational statement that ensured the satisfaction of all the boundary conditions (i.e. on both  $S_1$  and  $S_2$ ) and the equations of equilibrium, we conclude that (10) is a variational statement that would ensure the satisfaction of the equations of equilibrium in  $V$  and the boundary conditions on  $S_2$  only. Therefore the eigenfunctions we seek should satisfy the variational principle (10). It should also be noted that in this derivation no particular assumption was made regarding the constitutive relation for the elastic material except that it possessed a strain energy density function.

Let the stresses and the strains be represented by 1-D arrays as follows:

$$\left. \begin{array}{l} \sigma_1 = \sigma_{rr}; \sigma_2 = \sigma_{\theta\theta}; \sigma_3 = \sigma_{\phi\phi} \\ \sigma_4 = \sigma_{\theta\phi}; \sigma_5 = \sigma_{r\phi}; \sigma_6 = \sigma_{r\theta} \end{array} \right\} \quad (12)$$

$$\left. \begin{array}{l} \epsilon_1 = \epsilon_{rr}; \epsilon_2 = \epsilon_{\theta\theta}; \epsilon_3 = \epsilon_{\phi\phi} \\ \epsilon_4 = 2 \epsilon_{\theta\phi}; \epsilon_5 = 2 \epsilon_{r\phi}; \epsilon_6 = 2 \epsilon_{r\theta} \end{array} \right\} \quad (13)$$

The material constitutive relation is

$$\sigma_i = C_{ij} \epsilon_j \quad (14)$$

where  $C_{ij}$  is the material stiffness which satisfies

$$C_{ij} = C_{ji} \quad (15)$$

In equation (14) and in the following sections repeated indices imply summation unless otherwise stated.

As explained earlier,  $\Phi_u$ ,  $\Phi_{u_r}$ , ... are evaluated by using equation (4) and treating E as a function of  $\epsilon_{ij}$  and then using the chain rule. The results are:

$$\left. \begin{aligned} \Phi_u &= r(\sigma_2 + \sigma_3) \sin \theta \\ \Phi_{u_r} &= r^2 \sigma_1 \sin \theta \\ \Phi_{u_\theta} &= r \sigma_6 \sin \theta \\ \Phi_{u_\phi} &= r \sigma_5 \\ \Phi_v &= r(\sigma_3 \cos \theta - \sigma_6 \sin \theta) \\ \Phi_{v_r} &= r^2 \sigma_8 \sin \theta \\ \Phi_{v_\theta} &= r \sigma_2 \sin \theta \\ \Phi_{v_\phi} &= r \sigma_4 \\ \Phi_w &= -r(\sigma_4 \cos \theta - \sigma_5 \sin \theta) \\ \Phi_{w_r} &= r^2 \sigma_5 \sin \theta \\ \Phi_{w_\theta} &= r \sigma_4 \sin \theta \\ \Phi_{w_\phi} &= r \sigma_3 \end{aligned} \right\} \quad (16)$$

Now we can use the expressions in equation (1) for u, v and w. The strain-displacement relations yield:

$$\epsilon_i = r^{\lambda-1} \bar{\epsilon}_i, \quad i=1, \dots, 6 \quad (17)$$

where

$$\left. \begin{array}{l} \bar{\epsilon}_1 = \lambda f \\ \bar{\epsilon}_2 = g_\theta + f \\ \bar{\epsilon}_3 = f + g \cot \theta + g_\phi / \sin \theta \\ \bar{\epsilon}_4 = h_\theta - h \cot \theta + g_\phi / \sin \theta \\ \bar{\epsilon}_5 = (\lambda-1)h + f_\phi / \sin \theta \\ \bar{\epsilon}_6 = (\lambda-1)g + f_\theta \end{array} \right\} \quad (18)$$

In (18) subscripts  $\theta$  and  $\phi$  refer to differentiation with respect to these variables. Substitution of (17) into (14) gives:

$$\sigma_i = r^{\lambda-1} \bar{\sigma}_i, \quad i = 1, \dots, 6 \quad (19)$$

where

$$\bar{\sigma}_i = C_{ij} \bar{\epsilon}_j \quad (20)$$

It should be noted that in the case of a general anisotropic material,

$C_{ij} = C_{ij}(\theta, \phi)$  and therefore  $\sigma_i = \sigma_i(\theta, \phi)$ .

When (19) is substituted into (16) and then into (7) we get:

$$\delta \bar{U} = \int_V r^{2\lambda} \delta \tilde{U} dr \quad (21)$$

where

$$\delta \tilde{U} = \int_\theta \int_\phi \{ F \delta f + F^\theta \delta f_\theta + F^\phi \delta f_\phi + G \delta g + G^\theta \delta g_\theta + G^\phi \delta g_\phi + H \delta h + H^\theta \delta h_\theta + H^\phi \delta h_\phi \} d\theta d\phi \quad (22)$$

and

$$\left. \begin{array}{l} F = [\bar{\sigma}_2 + \bar{\sigma}_3 - (\lambda+1)\bar{\sigma}_1] \sin \theta \\ F^\theta = \bar{\sigma}_6 \sin \theta \\ F^\phi = \bar{\sigma}_5 \\ G = \bar{\sigma}_3 \cos \theta - (\lambda+2)\bar{\sigma}_6 \sin \theta \\ G^\theta = \bar{\sigma}_2 \sin \theta \\ G^\phi = \bar{\sigma}_4 \\ H = -\bar{\sigma}_4 \cos \theta - (\lambda+2)\bar{\sigma}_5 \sin \theta \end{array} \right\} \quad (23)$$

(23)  
cont'd

$$H^\theta = \bar{\sigma}_4 \sin \theta$$

$$H^\phi = \bar{\sigma}_3$$



Equation (21), when substituted into (10), yields the final variational principle for the present problem as

$$\delta \tilde{U} = 0 \quad \text{for all } \delta f, \delta g, \delta h \quad (24)$$

Bazant and Estensoro [8,9] who investigated the 3-D stress singularities in isotropic elastic materials using this approach have given the expressions for  $F$ ,  $F^\theta, \dots$  for isotropic materials. We have checked and verified that when  $C_{ij}$  is specialized to isotropic materials, the expressions given in (23) do in fact reduce to those given in [8,9] (after minor printing mistakes are corrected [9]).

## 2.2 DESCRETIZED FORMULATION.

To derive the expressions for a descretized (finite element) formulation let the area containing material bounded by the curve  $\psi(\theta, \phi) = 0$  on the  $(\theta, \phi)$  plane be denoted by  $A$  and let it be sub-divided into an  $n$  number of finite elements. The values of  $f(\theta, \phi)$ ,  $g(\theta, \phi)$  and  $h(\theta, \phi)$  are taken as the nodal degrees of freedom. We can express the integral  $\delta \tilde{U}$  of equation (22) as the sum of the same integral taken over each element (provided that the continuity conditions discussed below are satisfied). Hence

$$\delta \tilde{U} = \sum \delta \tilde{U}^{(m)} \quad (25)$$

where  $\delta \tilde{U}^{(m)}$  refers to the result of integrating the same integrand as that given for  $\delta \tilde{U}$  in equation (22) over the area of the  $m^{\text{th}}$  element,  $A^{(m)}$ .  $\sum$  in the above equation as well as in the following steps implies summation over all

n elements. Examination of the terms in the integrand of equation (22) shows that for equation (25) to hold f, g and h should be  $C^0$  over A (i.e. only the functions themselves need be continuous, not the derivatives). This justifies the choice of the values of the functions as the nodal degrees of freedom. The intra-element interpolations also need satisfy only function continuity along the inter-element boundaries.

Let  $\underline{x}$  be the vector of nodal degrees of freedom associated with a typical element and define interpolation functions  $\underline{L}(\theta, \phi)$ ,  $\underline{M}(\theta, \phi)$  and  $\underline{N}(\theta, \phi)$  by

$$\left. \begin{aligned} f(\theta, \phi) &= L^i(\theta, \phi) x_i \\ g(\theta, \phi) &= M^i(\theta, \phi) x_i \\ h(\theta, \phi) &= N^i(\theta, \phi) x_i \end{aligned} \right\} \quad (26)$$

In equation (26) as well as in the following steps superscript i on L, M or N and subscript i on  $x$  refer to the  $i^{\text{th}}$  entry in each vector. As has already been stated repeated indices imply summation.

Substitution of equation (26) into (18) gives

$$\bar{\epsilon}_i = E_{ij} x_j \quad (27)$$

with the 2-D array  $E_{ij}$  defined as

$$\left. \begin{aligned} E_{1j} &= \lambda L_j \\ E_{2j} &= M_\theta^j + L_\theta^j \\ E_{3j} &= L^j + M^j \cot \theta + N_\phi^j / \sin \theta \\ E_{4j} &= N_\theta^j - N^j \cot \theta + M_\phi^j / \sin \theta \\ E_{5j} &= (\lambda-1) N^j + L_\phi^j / \sin \theta \\ E_{6j} &= (\lambda-1) M^j + L_\theta^j \end{aligned} \right\} \quad (28)$$

where subscripts  $\theta$ ,  $\phi$  on  $L^j$ ,  $M^j$  and  $N^j$  refer to differentiation with respect to that variable. When equation (27) is substituted into (20) we get

$$\bar{\sigma}_i = S_{ij} x_j \quad (29)$$

where the 2-D array  $S_{ij}$  is given by

$$S_{ij} = C_{ik} E_{kj} \quad (30)$$

Now by substituting equation (29) into (23) we can define

$$\left. \begin{array}{l} F = P_i X_i \\ F^\theta = P^\theta_i X_i \\ F^\phi = P^\phi_i X_i \\ G = Q_i X_i \\ G^\theta = Q^\theta_i X_i \\ G^\phi = Q^\phi_i X_i \\ H = R_i X_i \\ H^\theta = R^\theta_i X_i \\ H^\phi = R^\phi_i X_i \end{array} \right\} \quad (31)$$

with

$$\left. \begin{array}{l} P_i = [S_{2i} + S_{3i} - (\lambda+1)S_{1i}] \sin \theta \\ P^\theta_i = S_{6i} \sin \theta \\ P^\phi_i = S_{5i} \\ Q_i = S_{3i} \cos \theta - (\lambda+2)S_{6i} \sin \theta \\ Q^\theta_i = S_{2i} \sin \theta \\ Q^\phi_i = S_{4i} \\ R_i = -S_{4i} \cos \theta - (\lambda+2)S_{5i} \sin \theta \\ R^\theta_i = S_{4i} \sin \theta \\ R^\phi_i = S_{3i} \end{array} \right\} \quad (32)$$

Using equations (26) and (31) in (22) and integrating over the area of the element  $A(m)$  we finally get

$$\delta U^{(m)} = \delta X_i K_{ij}^{(m)} X_j \quad (33)$$

where

$$K_{ij}^{(m)} = \iint_A^{(m)} \{ P_j L^i + P_j^\theta L_\theta^i + P_j^\phi L_\phi^i + Q_j M^i + Q_j^\theta M_\theta^i + Q_j^\phi M_\phi^i \\ + R_j N^i + R_j^\theta N_\theta^i + R_j^\phi N_\phi^i \} d\theta d\phi \quad (34)$$

In matrix notation (33) is

$$\delta \tilde{U}^{(m)} = \delta \tilde{X}^T \tilde{K}^{(m)} \tilde{X} \quad (35)$$

Let  $\tilde{X}^*$  be the vector of global degrees of freedom and let  $\tilde{X}$  be related to  $\tilde{X}^*$  through the connectivity matrix  $\tilde{B}^{(m)}$  so that

$$\tilde{X} = \tilde{B}^{(m)} \tilde{X}^* \quad (36)$$

When this is substituted into equation (35) we get

$$\delta \tilde{U}^{(m)} = \delta \tilde{X}^{*T} \tilde{B}^{(m)} \tilde{K}^{(m)} \tilde{B}^{(m)} \tilde{X}^* \quad (37)$$

With equations (25) and (37), the governing variational principle (24) can be expressed as

$$\delta \tilde{U} = \sum \delta \tilde{U}^{(m)} = \delta \tilde{X}^{*T} \tilde{K}^{(m)} \tilde{X}^* = 0 \quad \text{for all } \delta \tilde{X}^* \quad (38)$$

where

$$\tilde{K} = \sum \tilde{B}^{(m)} \tilde{K}^{(m)} \tilde{B}^{(m)} \quad (39)$$

For equation (38) to hold for all  $\delta \tilde{X}^*$  we require

$$\tilde{K} \tilde{X}^* = 0 \quad (40)$$

Equation (40) identifies  $\tilde{K}$  as being similar to the 'global stiffness matrix' in standard finite element analysis and it follows that  $\tilde{K}^{(m)}$  is similar to the 'element stiffness matrix'. Hereafter  $K$  and  $\tilde{K}^{(m)}$  will be referred to by those

names. It should be noted that equation (39) is only symbolic and in practice the formation of  $\underline{K}$  from  $\underline{K}^{(m)}$  is accomplished through the usual assembly procedures.

Elements of  $\underline{K}$  depend on  $\lambda$  and to derive a characteristic equation for  $\lambda$  we note that for equation (40) to have a non-trivial solution

$$\|\underline{K}\| = 0 \quad (41)$$

This provides the eigenequation for  $\lambda$ .

### 2.3 THE ELEMENT

The expressions needed for evaluating the element stiffness matrix have been given in the previous section. For actual numerical implementation of the scheme one has to decide on a particular 2-D element. Since only the functions  $f$ ,  $g$  and  $h$  are required to be continuous, any element type normally used in 2-D stress analysis can be picked for this purpose.

In [8,9] a 4-node quadrilateral based on the same variational principle has been used to investigate 3-D stress singularities in isotropic materials. The results showed fairly large errors and meshes with a substantial number of elements were required to achieve a reasonable degree of accuracy. However it was possible to exploit the convergence pattern of the results to extrapolate them and find accurate solutions. When a symmetry of the geometry and of the material property exist, one can make use of the symmetry by considering only one half of the problem. But in the case of a general anisotropic material such symmetry would be lacking and the full problem will have to be analysed. This will make it difficult to use very fine meshes and therefore it was decided to use a higher order element for the present study. It would enable reasonable accuracies to be realized without having to use a large number of elements.

The chosen element is an 8-node isoparametric quadrilateral with nodes at the four corners and the mid-sides. The interpolations are quadratic and curved sides are admissible. Following standard 2-D finite element procedures all integrations are performed numerically on a parent plane onto which the element is mapped as a unit square. This element is now standard and details of the interpolation functions and numerical integration are found in any standard text book on finite elements, (for example, see chapters 7 and 8 of [14]).

Numerical integration is performed using Gauss quadrature rule on a grid of  $n_G \times n_G$  integration stations. In a general anisotropic material the elements of the material stiffness matrix  $C_{ij}$  also are functions of  $\theta$  and  $\phi$  and at every integration station they too have to be evaluated. The transformation is that corresponding to a 4<sup>th</sup> order tensor and the transformation matrix contains terms like  $\cos \theta$ ,  $\cos \phi$ ,  $\sin \theta$  and  $\sin \phi$ . Therefore  $C_{ij}$  will display a strong dependence on these terms and their higher powers. The terms  $E_{ij}$  also contain these trigonometric functions. Examination of the expressions involved show that terms like  $1/\sin \theta$  also are present. This leads to some difficulties numerically in evaluating the integrals accurately especially in the region near the pole of the coordinate system where  $\theta \approx 0$ . Since a prior estimate of the number of integration stations is not possible, the choice of integration stations has to be based on numerical testing. In the following sections where test and example problems are presented, we will illustrate the effect of varying the number of Gauss integration stations and discuss the choice of optimal number of integration stations.

## 2.4 EVALUATION OF $\lambda$

The details of computing  $\lambda$  for a given problem is simple. The domain occupied by the material in the  $(\theta, \phi)$  plane is subdivided into a finite element mesh. For a particular value of  $\lambda$ , element stiffnesses are computed and are then assembled into the global stiffness matrix  $\tilde{K}$ . Boundary conditions are imposed by eliminating rows and columns corresponding to degrees of freedom prescribed to be zero in the global stiffness matrix. Finally  $\| \tilde{K} \|$  is computed. The eigenvalue  $\lambda$  (for which  $\| \tilde{K} \| = 0$ ) is determined by plotting  $\| \tilde{K} \|$  vs.  $\lambda$ . For the test problems and the example problems discussed herein these curves were smooth and no difficulties were encountered in implementing this scheme.

### 3. TEST PROBLEMS

The performance of the 8-node element was tested by using it to solve two different problems with known solutions. These tests and their results are described below.

#### 3.1 3-D CRACK IN ISOTROPIC MATERIALS

The problem of stress singularities at the tip of a quarter infinite crack in an isotropic half space with the crack front normal to the free surface, Fig. 2a, was first studied by Benthem [10]. Using a semi analytical-numerical technique he evaluated the eigenvalue  $\lambda$  corresponding to a state of symmetric deformation for different values of the Poisson's ratio  $\nu$ . These results were subsequently verified by Bazant and Estenssoro [9] who proposed the variational principle used in the present study and developed a 4-node quadrilateral element for isotropic materials. In addition they also reported the eigenvalues for antisymmetric deformations. Later Benthem [11] verified these results using a finite difference scheme. Another study of the same problem has been reported by Kawai et al. [13]. While confirming the results of [10] they also reported the detection of additional stronger singularities. But that has not been verified in subsequent work [9] and now it is generally believed that the results of Benthem [11] and Bazant and Estenssoro [9] are correct [3]. In our first test the 8-node element was used to solve the same problem and the results were compared against those from [9,11].

The domain of interest in the  $(\theta, \phi)$  plane is a rectangle bounded by  $\theta=0$ ,  $\theta=\pi/2$ ,  $\phi=0$  and  $\phi=\pi$ , Fig. 2b. Only one half of the problem was analysed using the symmetry of the geometry. The domain was sub-divided into  $(n_\theta \times n_\phi)$  elements;  $n_\theta$  in the  $\theta$  direction and  $n_\phi$  in the  $\phi$  direction. At nodes on the boundary AB corresponding to the plane of symmetry  $\phi=\pi$ , the symmetric or anti-

symmetric boundary conditions were imposed depending on the case to be analysed. The symmetric boundary conditions are:  $w=0$ ,  $\sigma_{\theta\phi}=0$ ,  $\sigma_{r\phi}=0$  and the anti-symmetric boundary conditions are:  $u=0$ ,  $v=0$ ,  $\sigma_{\phi\phi}=0$ . Of these only the displacement boundary conditions are imposed explicitly. The stress free conditions are the natural boundary conditions of the variational principle and will be automatically satisfied if the corresponding displacement component is not prescribed. No displacement boundary conditions are prescribed on the other boundaries (i.e. OA, BC and CO in Fig. 2b) so that the corresponding surfaces remain traction free.

The work of Bazant and Estenssoro [9] shows that the 4-node quadrilateral element based on the present variational principle would produce the same results as those reported in [10,11] for this problem. As the approaches used in [10,11] are quite different from that in [9] it strongly suggests that those results are accurate. Therefore it is reasonable to expect that the 8-node element too would yield the same results. The more important aspect of this test was to compare the errors and the convergence of the 8-node element against those for the 4-node element. However, the first task was to decide upon the number of integration stations  $n_G$  to be used for this problem and for that purpose one particular case (corresponding to  $\nu=0.3$  and anti-symmetric deformation) was run with varying values for  $n_G$ . The results are presented in Table 1. On the basis of the rapidity of convergence to a steady value  $n_G=4$  was chosen as the optimal order of integration for this problem and was used in the subsequent runs.

The results presented in Table 1 suggest that a mesh of (3x6) should produce values for  $\lambda$  within 1% of the 'correct' value. Therefore in the next step of computing values of  $\lambda$  corresponding to different values of  $\nu$  the mesh of (3x6) was used. As an additional check though, a mesh of (4x8) also was used. Subdi-

visions were made uniform since it is reported in [9] that non uniform grids are not more effective than uniform grids. The number of elements in the  $\phi$  direction ( $n_\phi$ ) was always kept equal to twice that in the  $\theta$  direction ( $n_\theta$ ) so that the finite elements would have equal side lengths on the  $(\theta, \phi)$  plane.

For the above two meshes and different values of  $\nu$ , the computed values of  $\lambda$  for both symmetric and anti-symmetric deformations are presented in Table 2. The corresponding 'extrapolated values' from [9] and the values from [11] are also presented in Table 2 for comparision and excellent agreement is evident. What is more important though is the remarkably rapid rate of convergence exhibited by the 8-node element when compared with that for the 4-node element. To see this the results in Table 2 have to be compared with those in Fig. 8 of [9]. Comparision should be based on the total number of degrees of freedom (which is the same as the total number of equations) because that is the primary factor that determines the computational effort involved. As a result of this rapid convergence the need to extrapolate the results using convergence characteristics reported in [9] can be eliminated and reasonably accurate results can be directly obtained from a relatively coarse finite element mesh.

### 3.2 AXISYMMETRIC NOTCH IN TRANSVERSELY ISOTROPIC MATERIAL

The second test problem was chosen with the intention of studying the performance of the element (and in fact of the whole finite element scheme) when the material is anisotropic. The geometry is assumed to be axisymmetric and the conical notch is defined by  $\theta = \theta_0$ , Fig. 3. The region  $0 \leq \theta \leq \theta_0$  is occupied by the material which is transversely isotropic with respect to the z axis. In [6] analytical solutions are obtained for this problem for both traction free and rigidly clamped boundary conditions on the surface  $\theta = \theta_0$ . When the material is transversely isotropic, there are five independent elastic constants

for  $C_{ij}$ . For a test problem we have selected the following special class of transversely isotropic materials in which  $C_{ij}$  depends on four parameters  $\mu$ ,  $\nu$ ,  $\beta$  and  $\gamma$ :

$$\left. \begin{aligned} C_{11} &= (\delta + 2\mu) \beta^2 \\ C_{33} &= (\delta + 2\mu) / \beta^2 \\ C_{44} &= \mu \\ C_{13} &= \delta \\ C_{11} - C_{12} &= 2\gamma\mu \end{aligned} \right\} \quad (42)$$

where

$$\delta = 2\mu\nu / (1-2\nu) \quad (43)$$

This class of materials has the property that the 'eigenvalues of the elasticity constants' are repeated [15]. Moreover, when  $\gamma = \beta = 1$  we have isotropic materials. We chose  $\theta_0 = 3\pi/4$  and considered the traction-free boundary condition.

In the  $(\theta, \phi)$  plane the material occupies a rectangular domain given by ( $0 \leq \theta \leq \theta_0$ ;  $0 \leq \phi \leq 2\pi$ ) with the two boundaries  $\phi=0$  and  $\phi=2\pi$  having the same displacements. In general the finite element mesh would have to cover this area. However, the axisymmetry of the present problem can be used to significantly reduce the magnitude of the computational effort. On any plane through the z axis symmetric boundary conditions (viz.  $w=0$ ,  $\sigma_{\theta\phi}=\sigma_{r\phi}=0$ ) should be satisfied. Further, the non-zero displacements  $u$  and  $v$  should be independent of  $\phi$ . This enables us to confine the analysis to just one strip of elements in the  $\theta$  direction. The number of elements in that strip is  $n_\theta$ . Through appropriate assembly procedures the same nodal degree of freedom is assigned to the value of  $f(\theta, \phi)$  or  $g(\theta, \phi)$  at all nodes at the same  $\phi$  level. Symmetric boundary conditions are prescribed at the two sides; and at the top (i.e. at  $\theta=0$ ) the axisym-

metric conditions (viz.  $u=0$ ,  $w=0$ ) are imposed. The bottom boundary  $\theta=\theta_0$  is left traction free. The width of the strip of elements is adjusted according to  $n_\theta$  so as to result in square elements.

The material constants  $C_{ij}$  can be normalized by dividing by  $\mu$ . Therefore the results would depend only on  $\nu$ ,  $\beta$  and  $\gamma$ . In the first case, for a particular set of their values ( $\nu=0.3$ ,  $\beta=1.5$ ,  $\gamma=0.5$ )  $\lambda$  was computed using different numbers of integration stations and different meshes. The results are presented in Table 3. As described in the case of test problem 1, in this case too an optimal value for  $n_G$  was selected as 4. A mesh with 4 elements gives results accurate within 0.1%. This combination was then used to compute values of  $\lambda$  corresponding to other values of  $\nu$ ,  $\beta$  and  $\gamma$  and the results are given in Table 4 along with the analytical solutions from [6]. The special case of  $\beta = \gamma = 1$  corresponds to isotropic materials and the value of  $\lambda$  for that case has been reported in [16]. The agreement between the finite element results and the analytical results is quite encouraging and reinforces the belief that the finite element scheme and the 8-node element would perform satisfactorily even in the case of anisotropic materials. Once again, the remarkable rapidity with which the results converge as evident from Table 3 should be noted.

#### 4. AN APPLICATION TO COMPOSITE MATERIALS

The use of light weight composite materials in industrial applications is steadily increasing. In areas where weight is a crucial factor such as space-craft designs, one would like to be able to exploit the strength of the materials to the fullest possible extent and the availability of relevant design information assumes great importance. Failure criteria are among those highly desired material parameters. In the case of laminated composites experimental observations indicate that failure may occur along the interface between the layers or transverse to the layers. It is well known that stress singularities occur at the free-edge of the interface between two dissimilar materials and they, no doubt, play an active role in initiating these failures. As such, development of failure criteria requires a sound understanding of the nature of stress singularities that would be present at the interface and it has been the subject of many recent investigations, (e.g. see [17-19]).

Consider the case where a transverse crack is already present at the free surface of a laminated composite. It may have resulted from a material imperfection or from a fabrication error. Or else it may have been initiated by the above mentioned free-edge stress singularities arising as a result of external loading. In Fig. 4 such a crack which is normal to and ends at the interfaces is shown by the shaded area. The presence of this crack would affect the local stress field and the nature of stress singularities. In fact it would give rise to a new stress singularity (i.e. in addition to those that would occur along free-edges such as MN) along the transverse crack edge MQ. A similar situation would occur with any other orientation of the crack, and in particular with a crack along the interface which could result from delamination. But for the purpose of the present discussion we shall confine our attention to the crack shown in Fig. 4. The singularity along MQ would now control, at least locally, the process of material failure and as such merits investigation.

Even though in principle the singularity at a point on MQ is 3-dimensional, as a first approximation its analysis may be reduced to a 2-dimensional problem provided that the point is sufficiently away from the free surface. This has been done in [19] and also given therein is an account of relevant previous work on 2-dimensional problems. In the present study we direct our attention to the nature of the 3-dimensional stress singularity at the point M.

In the immediate neighbourhood of the point M the problem of stress singularities is very much similar to the problem of quarter infinite crack in a half space discussed in Section 3 except for the fact that the material is neither homogeneous nor isotropic. The region ( $x < 0, z \geq 0$ ) is occupied by the material of layer 2 while the regions ( $x > 0, y > 0, z \geq 0$ ) and ( $x > 0, y < 0, z \geq 0$ ) are occupied by the material of layer 1. It should also be noted that even though in Section 3 it was possible to confine the analysis to only one half of the problem by exploiting symmetry, in the present case the material will not exhibit such symmetry in general and therefore the full problem has to be analysed. Once these points are identified the analysis can be performed in a manner quite parallel to that employed previously.

The domain occupied by the material in  $(\theta, \phi)$  plane is the rectangle ( $0 \leq \theta \leq \pi/2, 0 < \phi < 2\pi$ ). In this, the two regions ( $0 \leq \theta \leq \pi/2, 0 < \phi < \pi/2$ ) and ( $0 \leq \theta \leq \pi/2, 3\pi/2 < \phi < 2\pi$ ) correspond to material 1 and the region ( $0 \leq \theta \leq \pi/2, \pi/2 < \phi < 3\pi/2$ ) corresponds to material 2. The entire region is subdivided into ( $n_\theta \times n_\phi$ ) finite elements. For this problem  $n_\phi$  was made equal to  $4n_\theta$  so that square elements would result. It also ensures that each element would lie entirely within one material. During the computation care has been exercised in assigning the correct material properties to each finite element.

The remaining steps are routine. The element stiffnesses are computed for a given  $\lambda$  and assembled into the global stiffness matrix. The boundary conditions

are all traction free conditions and none needs to be imposed explicitly. The eigenvalue  $\lambda$  is obtained by plotting the determinant of the global stiffness matrix against corresponding value of  $\lambda$ .

As explained in Section 3 the first task is to select the optimal order of Gauss integration  $n_G$ . Like in the test problems, this is done by carrying out numerical tests to study the convergence of the results as the mesh is refined and  $n_G$  is varied. Once optimal  $n_G$  is selected a mesh that could be expected to yield 'sufficiently accurate' results can be selected and used for analysing the remaining cases of the same type. What is 'sufficiently accurate' is, of course, subjective and would depend to a great extent on the intended application of the result. It would also be controlled by physical limitations of available computing capacity.

For the purpose of a numerical example, we assume that each layer in the composite is made of a fiber reinforced material which can be regarded as an orthotropic material whose material symmetry is with respect to the  $x_1$ ,  $x_2$ ,  $x_3$  axes where  $x_1=x$  and  $x_3$  axis is the fiber direction which makes an angle  $\alpha$  with the negative  $y$  axis as shown in Fig. 4. We further assume that each layer is made of the same material although the ply angle  $\alpha$  may vary from layer to layer. The value of  $\alpha$  corresponding to layer 1 is  $\alpha_1$ , and that corresponding to layer 2 is  $\alpha_2$ . Referring to the  $(x_1, x_2, x_3)$  axes let the orthotropic material have the following material properties corresponding to T300/5208 graphite/epoxy given in [20]. This is the same as the material referred to as composite T in [18,19].

$$\left. \begin{array}{l} E_1 = E_2 = 1.54 \times 10^6 \text{ psi} \\ E_3 = 22.0 \times 10^6 \text{ psi} \\ G_{12} = G_{23} = G_{31} = 0.81 \times 10^6 \text{ psi} \\ \nu_{21} = \nu_{31} = \nu_{32} = 0.28 \end{array} \right\} \quad (44)$$

In the above equation  $E_i$  are the Young's moduli,  $G_{ij}$  are the shear moduli and  $\nu_{ij}$  are the Poisson's ratios [21]. They can be used to compute the material compliance matrix [21,22] which when inverted using the relations given in [21] yields the material stiffness matrix referred to the  $(x_1, x_2, x_3)$  axes. Then the material stiffness matrix  $C_{ij}$  referred to the  $(x, y, z)$  axes can be obtained by an appropriate co-ordinate transformation. The use of ply angle  $\alpha_1$  will result in  $C_{ij}$  corresponding to material 1 while  $\alpha_2$  will result in  $C_{ij}$  for material 2.

For the purpose of selecting an optimal value for  $n_G$  we used the particular case with  $\alpha_1 = \pi/2$ ,  $\alpha_2 = 0$ . This choice restored material symmetry with respect to the  $y=0$  plane and thus allowed the analysis of only one half of the problem as in Section 3. That way the refinement of the mesh could be carried further than it would have been possible if the full problem had to be analysed. Attention was focused only on the smallest admissible value of  $\lambda$ . The results are presented in Table 5. On the basis of rapid convergence to a steady value  $n_G = 6$  was chosen as being optimal for this type of problem. The need for more integration stations than that required in the isotropic case discussed in Section 3 is perhaps a reflection of the higher degree of anisotropy involved. However, examination of the results in Table 5 indicate that even in this highly anisotropic problem the numerical scheme performs satisfactorily.

A mesh of  $(3 \times 12)$  was selected for use in analysing other  $(\alpha_1/\alpha_2)$  combinations. They would lack the material symmetry about the plane  $y=0$  required to confine the analysis to one half of the problem and would necessitate the analysis of the full problem. The available computing capacity did not permit the use of a more refined mesh. However, based on the results of the above test problem and also on the convergence pattern displayed by the results corresponding to other ply angle combinations we feel that the results from the  $(3 \times 12)$

mesh would be accurate to within at least 2%. In fact in most of the cases the error would be less than 1%. Proper verification of that estimate requires a reliable analytical result or at least a result from a different numerical procedure either of which to the authors' knowledge is not available as yet. The results from a mesh of (3x12) for different ply angle combinations are presented in Table 6. For comparision, in the same table we have provided within parenthesis the results from a mesh of (2x8). The small differences between the two sets of results lend support to the belief that the results are reasonably accurate. In view of the symmetry property that the  $\lambda$  corresponding to  $(\alpha_1/\alpha_2)$  is the same as that for  $(-\alpha_1/-\alpha_2)$  only the values of  $\lambda$  for  $0 \leq \alpha_1 \leq \pi/2$  are presented. They vary from 0.3016 (for 0/90 combination) to 0.4572 (for 90/60 combination). The strongest singularity occurs for the combination (0/90) and the corresponding order of stress singularity,  $1-\lambda$ , is -0.6984. In [19] the two-dimensional singularity at a point sufficiently away from the free surface was studied and it is shown that the strongest singularity in that case also occurs for the (0/90) combination.

## 5. STRESS SINGULARITIES AT OTHER THREE-DIMENSIONAL CORNERS

As a further example, in this section the present numerical scheme is used to investigate the possible occurrence of stress singularities in other 3-D corners. The problem of a corner formed by three mutually perpendicular planes is considered in the computations. The three planes are defined by  $\phi = 0$ ;  $\phi = \pi/2$  and  $\theta = \pi/2$ . (See Figure 5). Two different situations arise depending on which part is occupied by material and which part is void. Let the region ( $0 \leq \phi \leq \pi/2$ ,  $0 \leq \theta \leq \pi/2$ ) be denoted by R. One problem is when R is void and the rest of the space is occupied by the material. Hereafter it will be referred to as the 'exterior problem'. The other problem arises when the situation is reversed, i.e., R is occupied by the material while the rest is void. It will be referred to as the 'interior problem'.

Two materials are used in the sample computations: isotropic material (with Poisson's ratios of 0 and 0.3) and the material referred to as composite-T in Section 4 with properties given by equation (44). In the latter case the  $x_3$  axis is taken to be in the z direction so that material properties are rotationally symmetric about the z axis. This enables the analysis to be confined to one half of the problem and be performed separately for symmetric and antisymmetric modes of deformation.

### 5.1 EXTERIOR PROBLEM

One half of the domain of interest is shown in Figure 6(a). The number of elements in the  $\theta$  direction between 0 and  $\pi/2$  is the same as that between  $\pi/2$  and  $\pi$  and is denoted by  $n_\theta$ . The number of elements in the  $\phi$  direction between 0 and  $\pi/4$  is  $n_{\phi 1}$  while that between  $\pi/4$  and  $\pi$  is  $n_{\phi 2}$ . In order to have square elements on the  $\theta$ - $\phi$  plane the ratio  $n_\theta:n_{\phi 1}:n_{\phi 2}$  was maintained at 2:1:3.

The coarse mesh had  $(n_\theta, n_{\phi 1}, n_{\phi 2}) = (2, 1, 3)$  and the refined mesh  $(4, 2, 6)$ . Based on the experience gained from the computations of the previous problems it is believed that the latter mesh would produce results within 2% of the exact value. However the large size of the domain prevented any further refinements. The coarse mesh was first used to scan the real axis from 0 to 1.0 in search of a root  $\lambda$ . When one was located the refined mesh was used to compute its value more accurately. Previous experience suggested that  $n_G = 5$  should be adequate (where  $n_G$  is the number of Gauss integration stations). But for purposes of comparison calculations were performed using other values of  $n_G$  also. The results obtained for both isotropic and composite-T materials are presented in Table 7. In each case two symmetric and one anti-symmetric roots were observed on the real axis between 0 and 1.0. They all would give rise to stress singularities.

## 5.2 INTERIOR PROBLEM

Shown in Figure 6(b) is one half of the domain of interest for this problem on the  $\theta$ - $\phi$  plane. The number of elements in the  $\theta$  direction is  $n_\theta$  and that in the  $\phi$  direction is  $n_\phi$ . Ratio  $n_\theta:n_\phi$  was maintained at 2:1 so that square elements would result. In order to obtain the same size of elements as in the exterior problem  $(n_\theta, n_\phi) = (2, 1)$  was used for the coarse mesh while  $(4, 2)$  was planned for the refined mesh. However in the cases of both isotropic and composite-T materials a search using the coarse mesh revealed that there are no real roots of  $\lambda$  capable of causing stress singularities (i.e. between 0 and 1.0).

Attention was then focused on complex roots of  $\lambda$  to see whether there exists a  $\lambda$  whose real part is between 0 and 1.0. Computations were carried out using complex arithmetic and appropriate changes of the relevant variables from real

to complex. A rectangular region on the complex  $\lambda$  plane was scanned for roots. The search was performed by subdividing the region into a grid of small rectangles and then checking each of them to see whether a line corresponding to  $\text{Re}(\underline{\lambda}) = 0$  and/or  $\text{Im}(\underline{\lambda}) = 0$  would be present inside it. ( $\text{Re}$  and  $\text{Im}$  stand for the Real part and the Imaginary part respectively). This was determined by comparing the signs of the relevant quantity (i.e. either  $\text{Re}(\underline{\lambda})$  or  $\text{Im}(\underline{\lambda})$  as the case may be) at the four corners. If the sign changes among the four corners then it would be concluded that the corresponding line passes through the rectangle. By searching each small rectangle this way, it was possible to trace the locus of the lines  $\text{Re}(\underline{\lambda})=0$  and  $\text{Im}(\underline{\lambda})=0$ . Where they intersect is a root of  $\lambda$ . To illustrate the type of plot one would obtain, the results corresponding to composite-T material are given in Figures 7 and 8. Within the region scanned no roots capable of causing stress singularities were found even though some roots, both real and complex, were present in the region  $\text{Re}(\lambda) > 1.0$ . (Note that  $\lambda = 0$  corresponds to a rigid body translation while  $\lambda = 1$  produces a rigid body rotation and both of them produce no stresses). In the case of isotropic materials with  $\nu=0$  and  $0.3$  a similar situation prevailed. Corresponding plots of  $\text{Re}(\underline{\lambda})=0$  and  $\text{Im}(\underline{\lambda})=0$  were qualitatively similar to Figs. 7 and 8 and hence are not presented here. They can be found in [23].

## 6. CONCLUDING REMARKS

Assuming that the displacements in an anisotropic material is proportional to  $r^\lambda$  a finite element scheme is proposed to determine the eigenvalue  $\lambda$ . Since the stress is proportional to  $kr^{\lambda-1}$  where  $k$  is the proportionality factor, the stress is singular when  $\text{Re}(\lambda) < 1$ .  $\lambda$  is a root of the determinant of the matrix  $\tilde{K}$  in Eq. (40). The proportionality factor  $k$  has to be determined by considering the complete boundary conditions which include the boundary  $S$ , in Fig. 1. If  $k$  happens to be zero, there is no stress singularity at  $r = 0$  even if  $\text{Re}(\lambda) < 1$ . Thus the existence of a singularity is not certain until the complete boundary conditions are considered. If a singularity exists, the solution obtained here provides the order of stress singularity and, if one desires, the stress distribution near  $r = 0$  except the proportionality factor  $k$ .

Complications arise when  $\lambda$  is a multiple root of the determinant of  $\tilde{K}$ . The related problem for two dimensional cases has been investigated in [24,25] for isotropic materials and in [26] for anisotropic materials. It was shown that in addition to the  $r^{\lambda-1}$  singularity the stress may have the  $r^{\lambda-1} (\ln r)$  singularity. The conditions for which the stress has the  $r^{\lambda-1} (\ln r)$  singularity were given in [24]. The same conditions apply to the matrix  $\tilde{K}$  even though our problem is a three-dimensional one. No multiple roots are found in the examples presented here nor in other three-dimensional problems reported in the literature except in [6]. Even in the case of multiple roots of  $\tilde{K}$ , if the curves  $\text{Re}(\tilde{K})=0$  and  $\text{Im}(\tilde{K})=0$  are plotted on the complex plane as in Figs. 7 and 8, a root of multiplicity  $m$  would present itself as a common point of intersection of  $m$  curves of  $\text{Re}(\tilde{K})=0$  and  $m$  curves of  $\text{Im}(\tilde{K})=0$ .

Another complication arises when the conical wedge surface  $S_1$ , in Fig. 1, is not traction free and the matrix  $\tilde{K}$  is singular. In this case the right hand side of Eq. (40) is non-zero and a solution may not exist. A modified solution would give a singularity of the form  $k^*(\ln r)$  in which  $k^*$  is a constant. The related problem for two-dimensional cases has been studied in [27-29] for isotropic materials and in [30] for anisotropic materials. It should be pointed out that, unlike the constant  $k$  mentioned earlier which is indeterminate until the complete boundary conditions are considered,  $k^*$  here can be determined without solving the complete boundary value problem [30].

## REFERENCES

- [1] Sih, G.C., "A Review of the Three Dimensional Stress Problem for a Cracked Plate," *Int. J. Fracture Mech.*, 9, 39-61 (1971)
- [2] Kassir, M.K. and Sih, G.C., "Mechanics of Fracture 2 - Three Dimensional Crack Problems," Noordhoff International Publishing, Leyden, (1975)
- [3] Erdogan, F., "Stress Intensity Factors," *J. App. Mech.*, 50, 992-1002 (1983)
- [4] Parihar, K.S. and Keer, L.M., "The Singularity at the Corner of a Wedge-shaped Crack or Inclusion," *J. App. Mech.*, 45, 791-796 (1978)
- [5] Parihar, K.S. and Keer, L.M., "The Singularity at the Apex of a Bonded Wedge-shaped Stamp," *J. App. Mech.*, 46, 577-580 (1979)
- [6] Somaratna, Nihal and Ting, T.C.T., "Three Dimensional Stress Singularities at Conical Notches and Inclusions in Transversely Isotropic Materials," *J. App. Mech.*, 53, to appear (1986)
- [7] Bazant, Z.P., "Three-Dimensional Harmonic Functions Near Termination or Intersection of Gradient Singularity Lines: A General Numerical Method," *Int. J. Eng. Sci.*, 12, 221-243 (1974)
- [8] Bazant, Z.P. and Estenssoro, L.F., "General Numerical Method for Three Dimensional Singularities in Cracked or Notched Elastic Solids," *Fracture 1977*, Proc. 4<sup>th</sup> Int. Conf. Fracture, edited by Taplin, D.M.R., Univ. of Waterloo, Ontario, Canada, 1977, vol. 3, pp 371-385.
- [9] Bazant, Z.P. and Estenssoro, L.F., "Surface Singularity and Crack Propagation," *Int. J. Solids Structures*, 15, 405-426 (1979). See also "Erratum," in 19, 661 (1983)
- [10] Benthem, J.P., "State of Stress at the Vertex of a Quarter-Infinite Crack in a Half Space," *Int. J. Solids Structures*, 13, 479-492 (1977)
- [11] Benthem, J.P., "The Quarter-Infinite Crack in a Half Space; Alternative and Additional Solutions," *Int. J. Solids Structures*, 16, 119-130 (1980)
- [12] Benthem, J.P., "On an Inversion Theorem for Conical Regions in Elasticity Theory," *J. Elasticity*, 9, 159-169 (1979)
- [13] Kawai, T., Fujitani, Y. and Kumagai, K., "Analysis of Singularity at the Root of the Surface Crack Problem," Proc. Int. Conf. Fracture Mech. and Tech., edited by Sih, G.C. and Chow, C.L., vol II, pp 1157-1163 (1977)
- [14] Zienkiewicz, O.Z., "The Finite Element Method," 3<sup>rd</sup> ed., McGraw-Hill, London, 1977

- [15] Ting, T.C.T., Jin, Yijian and Chou, S.C., "Eigenfunctions at a Singular Point in Transversely Isotropic Materials Under Axisymmetric Deformations," *J. Appl. Mech.*, to appear (1985).
- [16] Bazant Z.P. and Keer, L.M., "Singularities of Elastic Stresses and of Harmonic Functions at Conical Notches and Inclusions," *Int. J. Solids Structures*, 10, 957-964 (1974)
- [17] Wang, S.S. and Choi, I., "Boundary Layer Effects in Composite Laminates," Parts 1 and 2, *J. App. Mech.*, 49, 541-560 (1982)
- [18] Zwiers, R.I., Ting, T.C.T. and Spilker, R.L., "On the Logarithmic Singularity of Free-edge Stress in Laminated Composites Under Uniform Extension," *J. App. Mech.*, 49, 561-569 (1982)
- [19] Ting, T.C.T. and Hoang, P.H., "Singularities at the Tip of a Crack Normal to the Interface of an Anisotropic Layered Composite," *Int. J. Solids Structures*, 20, 439-454 (1984)
- [20] Chou, S.C., "Delamination of T300/5208 Graphite/Epoxy Laminates," in Fracture of Composite Materials, edited by Sih, G.C. and Tamuzs, V.P., Nijhoff, Amsterdam, pp 247-263 (1982)
- [21] Jones R.M., "Mechanics of Composite Materials," McGraw-Hill, New York, 1975
- [22] Christensen, R.M., "Mechanics of Composite Materials," Wiley-Interscience, New York, 1979
- [23] Somaratna, Nihal, "Three-Dimensional Stress Singularities in Anisotropic Materials and Composites," Ph.D. Thesis, University of Illinois at Chicago, 1985.
- [24] Dempsey, J. P. and Sinclair, G. B., "Stress Singularities in the Plane Elasticity of the Composite Wedge," *J. Elasticity*, 9, 373-391 (1979).
- [25] Dempsey, J. P. and Sinclair, G. B., "On the Singular Behavior at the Vertex of a Bi-Material Wedge," *J. Elasticity*, 11, 317-327 (1981).
- [26] Ting, T. C. T. and Chou, S. C., "Edge Singularities in Anisotropic Composites," *Int. J. Solids Structures*, 17, 1057-1068 (1981).
- [27] Dempsey, J. P., "The Wedge Subjected to Traction: A Paradox Resolved," *J. Elasticity*, 11, 1-10 (1981).
- [28] Ting, T. C. T., "The Wedge Subjected to Traction: A Paradox Re-Examined," *J. Elasticity*, 14, 235-247 (1984).
- [29] Ting, T. C. T. and Chou, S. C., "Logarithmic Singularity of an Elastic Composite Wedge Subjected to Out-of-the-Plane Extensional Strain," *J. Theoretical and Applied Fracture Mechanics*, 4, No. 3, to appear (1985).
- [30] Zwiers, R. I., Ting, T. C. T. and Spilker, R. L. "On the Logarithmic Singularity of Free-Edge Stresses in Laminated Composites Under Uniform Extension," *J. Appl. Mech.*, 49, 561-569 (1982).

## Appendix A

### LIST OF COMPUTER PROGRAMS DEVELOPED FOR THIS STUDY

#### (1) Program: CON.NOTCH

This program is for analysing the possible stress singularities at the apex of conical regions in transversely isotropic materials using 8-node quadrilateral finite elements. The conical region can be defined either as having one conical boundary or as having two conical boundaries with material in between them. Either traction free or rigidly clamped conditions can be imposed on each boundary. The user has control over the number of elements and the order of integration. The program can be used either to locate a real root in a specified interval on the real axis or to compute the determinants corresponding to given real values of  $\lambda$ .

#### (2) Program: D3.CRACK.HALF

This is for the analysis of possible stress singularity at the tip of the transverse crack in a composite laminate shown in Fig. 4. Material properties are assumed to be such that there is symmetry and only one half of the problem is analysed. 8-node quadrilateral finite elements are used. The user can vary the mesh details and the order of Gauss integration. The program is capable of either searching for a real root within a given interval of the real axis to a specified accuracy or of just computing the determinants for specified real values of  $\lambda$ .

The same program can be used to analyse the 3-D crack in an isotropic half space also by assigning isotropic material properties to both layers of the composite.

(3) Program: D3.CRACK.FULL

This is for the analysis of possible 3-D stress singularities at the tip of a crack in a laminated composite. No material property symmetries are assumed and the full problem is analysed. The crack can be either normal to the interface or along the interface. Mesh is generated using 8-node elements. Mesh details and the order of Gauss integration are user definable. The program can either search for a real root in a given interval of the real axis to a specified accuracy or just compute the determinants corresponding to given real values of  $\lambda$ .

(4) Program: D3.CORNER.EXT

The exterior problem for a 3-D corner formed by 3 mutually perpendicular planes is analysed for the possible occurrence of stress singularities by this program. Mesh is generated for 8-node quadrilateral elements. Mesh parameters and the order of Gauss integration are user definable. Material is required to have properties symmetric with respect to the plane of geometric symmetry for the problem. Analysis is performed for either the symmetric or anti-symmetric mode and the program can either search for a real root within a specified region on the real axis to a specified accuracy or compute the determinants corresponding to given real values of  $\lambda$ .

(5) Program: D3.CORNER.INT

Similar to D3.CORNER.EXT except that this analyses the interior problem.

(6) Program: D3.CORNER.INT.CMPLX

Similar to D3.CORNER.INT except that the search for a root is carried out on the complex plane. Program produces the plots of the locii of  $\text{Re}(\|K\|) = 0$  and of  $\text{Im}(\|K\|) = 0$  in a specified region on the complex plane. Points of intersection of the two types of lines indicate locations of roots. An option to refine the root upto a specified accuracy also is available.

Number of Gauss Integration Stations $n_G$	Mesh* $n_\theta \times n_\phi$ (Total number of DOF)		
	2 x 4 (111)	3 x 6 (219)	4 x 8 (363)
3	0.3890	0.3883	0.3879
4	0.3946	0.3912	0.3911
5	0.3970	0.3929	0.3920
6	0.3991	0.3941	0.3932
8	0.4014	0.3955	0.3943
10	0.4029	0.3964	0.3950

\*Mesh is for one half of the problem.

Table 1 Values of  $\lambda$  for 3-D crack, Fig. 2a, in isotropic half space under an anti-symmetric deformation;  $v = 0.3$ .

value of $v$	Symmetric Deformation				Anti-symmetric Deformation			
	8-node element $n_G = 4$		from Bazant & Estenssoro [9]	from Benthem [11]	8-node element $n_G = 4$		from Bazant & Estenssoro [9]	from Benthem [11]
	mesh (3x6)	mesh (4x8)			mesh (3x6)	mesh (4x8)		
0	0.5010	0.5003	0.5	0.5	0.4985	0.4983	0.5	0.5
0.1	0.5107	0.5099	-	-	0.4492	0.4492	0.452	-
0.15	0.5173	0.5166	0.5164	0.5164	0.4316	0.4315	0.435	0.4332
0.3	0.5487	0.5478	0.5477	0.5477	0.3912	0.3911	0.402	0.3927
0.4	0.5883	0.5869	0.5868	0.5868	0.3703	0.3701	0.396	0.3714

**Table 2** Comparison of  $\lambda$  for 3-D crack, Fig. 2a,  
in isotropic materials using the present  
8-node element with those reported in [9,11].

Number of Gauss Integration Stations $n_G$	Number of Elements $n_\theta$				
	2	3	4	5	6
3	0.5999	0.5309	0.5292	0.5299	0.5298
4	0.5881	0.5306	0.5293	0.5299	0.5298
5	0.5880	0.5307	0.5293	0.5299	0.5298

Table 3 Values of  $\lambda$  for a conical notch (Fig. 3,  $\theta_0 = 3\pi/4$ ) in a transversely isotropic material ( $v = 0.3$ ,  $\beta = 1.5$ ,  $\mu = 1$ ,  $\gamma = 0.5$ ) using 8-node element with different numbers of Gauss integration stations and different meshes. Exact solution is  $\lambda = 0.5296$  [6].

Material Properties			Using 8-node finite elements $n_g=4; n_G=4$	Analytical solution from [6]
$\nu$	$\beta$	$\gamma$		
0.3	1.0	1.0	0.8014	0.8012*
	1.0	2.0	0.9445	0.9437
	1.5	0.5	0.5293	0.5296
	1.5	2.0	0.8529	0.8533
	0.5	0.5	0.9160	0.9131

\*this case corresponds to isotropic material and agrees with the analytical solution for isotropic cones reported in [16]

**Table 4** Comparison of  $\lambda$  for the conical notch, Fig. 3, in a transversely isotropic material using 8-node finite element with the analytical solution reported in [6].

Number of Gauss Integration Stations $n_G$	Mesh* $n_\theta \times n_\phi$			
	2x8	3x12	4x16	5x20
3	0.4220	0.4353	0.4393	0.4412
4	0.4394	0.4426	0.4448	0.4458
5	0.4448	0.4469	0.4482	0.4484
6	0.4487	0.4498	0.4505	0.4502
8	0.4520	0.4533	0.4533	0.4524
10	0.4555	0.4555	0.4550	0.4538
16	0.4597	0.4589	0.4578	0.4560
24	0.4623	0.4611	0.4595	0.4575

\*only one half of this mesh was analysed by using symmetry

Table 5 Values of  $\lambda$  for (90/0) composite, Fig. 4, for varying number of Gauss integration stations and different meshes.

$\alpha_1$ $\alpha_2$	0°	30°	60°	90°
-60°		0.4048 (0.4089)	0.4416 (0.4494)	
-30°		0.3881 (0.3904)	0.4352 (0.4377)	
0°	0.3860 (0.3909)	0.3872 (0.3914)	0.4128 (0.4190)	0.4497 (0.4484)
30°	0.3514 (0.3557)	0.3911 (0.3974)	0.4020 (0.4091)	0.4477 (0.4463)
60°	0.3171 (0.3181)	0.4067 (0.4128)	0.4264 (0.4356)	0.4572 (0.4602)
90°	0.3016 (0.2998)	0.4115 (0.4206)	0.4293 (0.4362)	0.4550 (0.4549)

Table 6 Values of smallest  $\lambda$  for  $(\alpha_1/\alpha_2)$  composite,  
Fig. 4, obtained from a (3x12) mesh.  $\lambda$  obtained  
from a (2x8) mesh are shown in parentheses.

Mode	Number of Gauss Integration Stations $n_G$	Material		
		Isotropic $\nu = 0$	Isotropic $\nu = 0.3$	Composite -T
Symmetric	5	0.7118 (0.7254)	0.7660 (0.7803)	0.7312 (0.7457)
	10	0.7122 (0.7269)	0.7668 (0.7824)	0.7315 (0.7440)
Symmetric	5	0.8554 (0.8643)	0.7805 (0.7928)	0.8157 (0.8350)
	10	0.8559 (0.8654)	0.7809 (0.7934)	0.8165 (0.8356)
Anti-symm.	5	0.7140 (0.7294)	0.7667 (0.7807)	0.7623 (0.7680)
	10	0.7141 (0.7301)	0.7671 (0.7823)	0.7663 (0.7744)

Table 7 Values of real  $\lambda$  within (0, 1.0) for 3-D corner exterior problem, Fig. 5a, computed on a (4,2,6) mesh. Results from a (2,1,3) mesh are shown in parentheses.

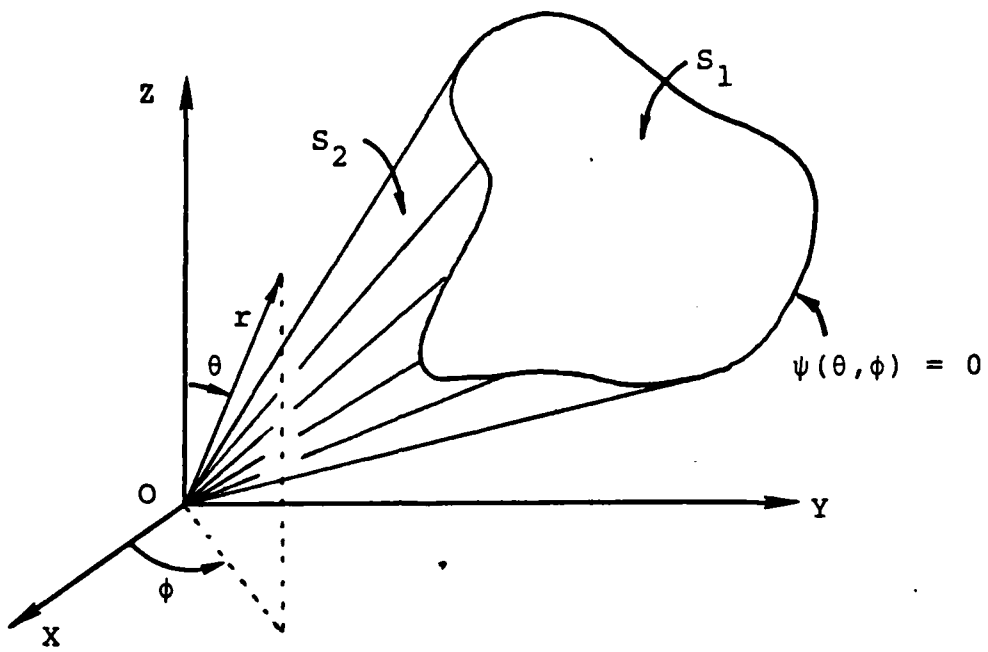


Fig. 1 Three dimensional conical notch/  
inclusion and the associated  
spherical coordinate system

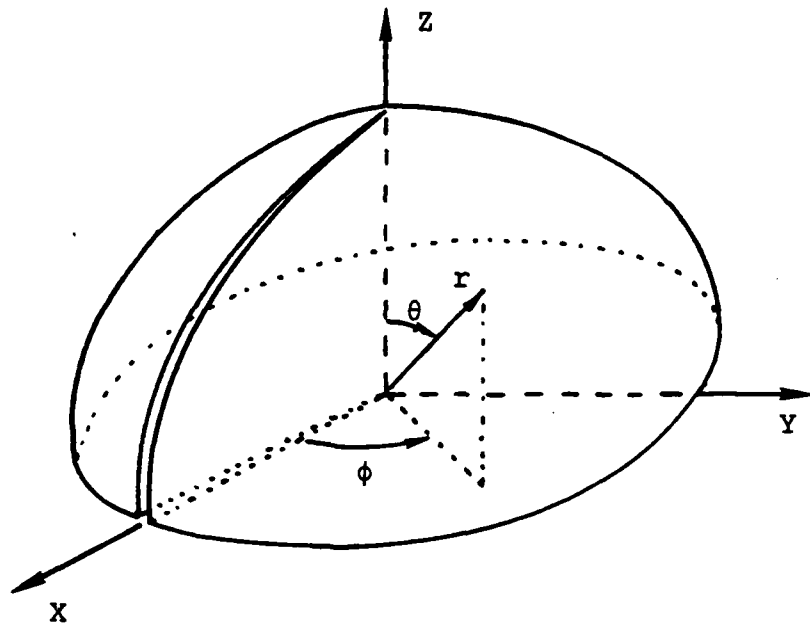


Fig. 2a Quarter-infinite crack in half space.  
Material is in  $0 \leq \theta \leq \pi/2$ .  
Free surface is  $\theta = \pi/2$  while crack  
surfaces are  $\phi = 0$  and  $2\pi$ .

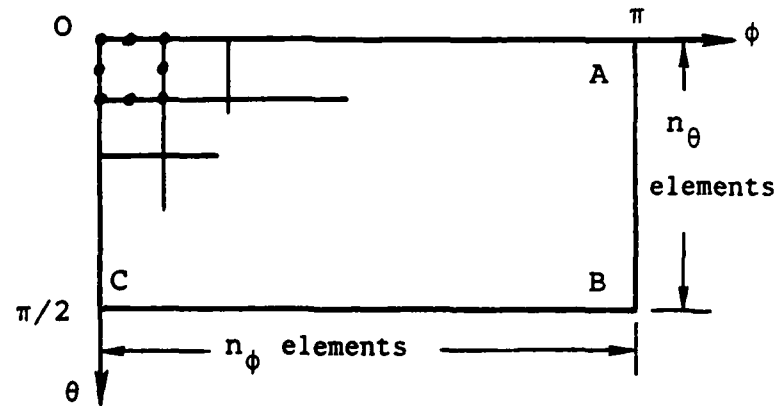


Fig. 2b Mesh for half of the problem with a  
typical 8-node element.

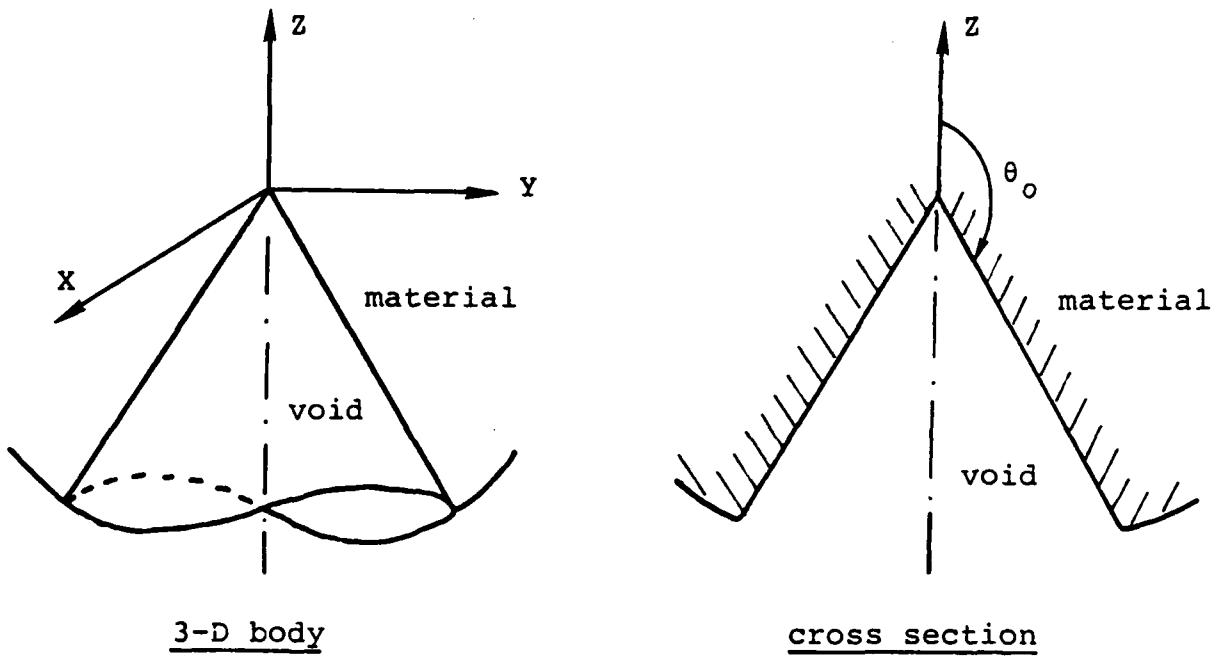
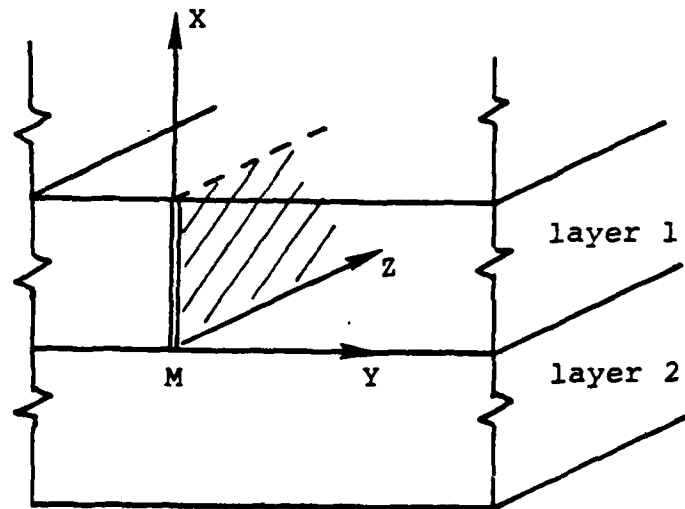
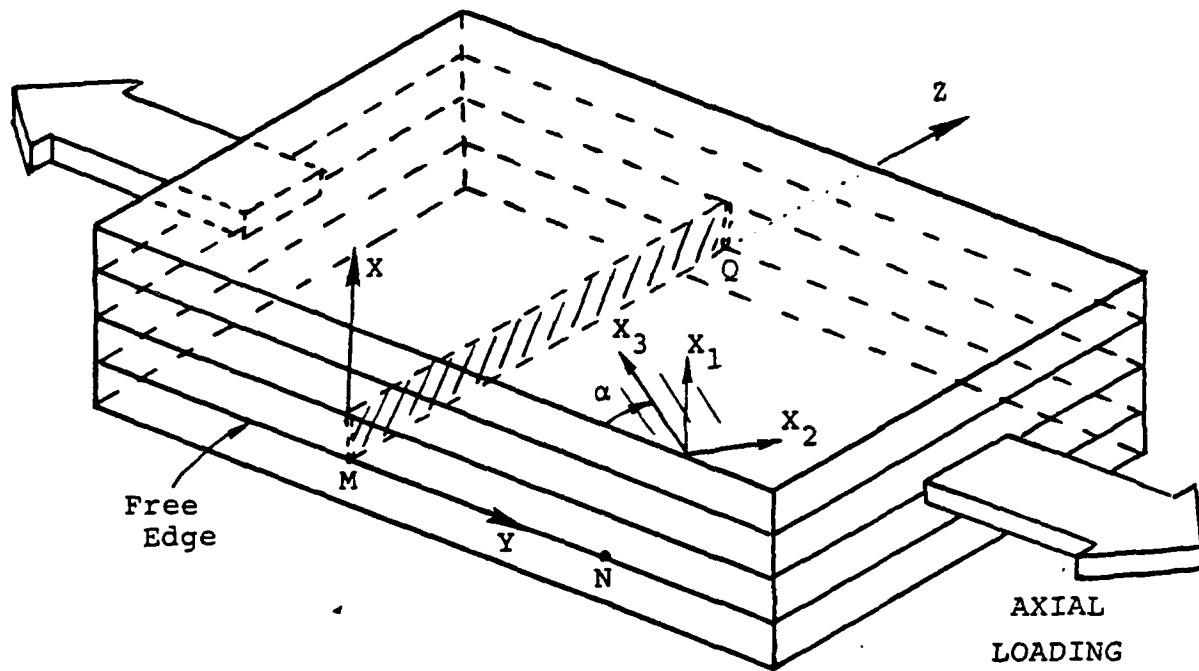
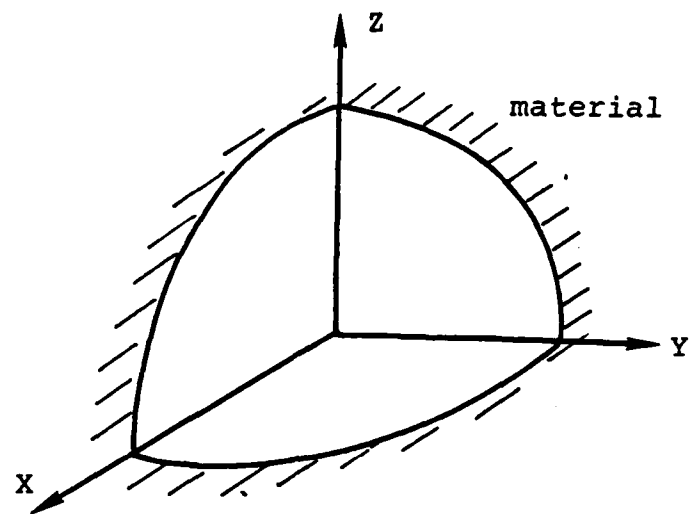


Fig. 3 Axisymmetric conical notch

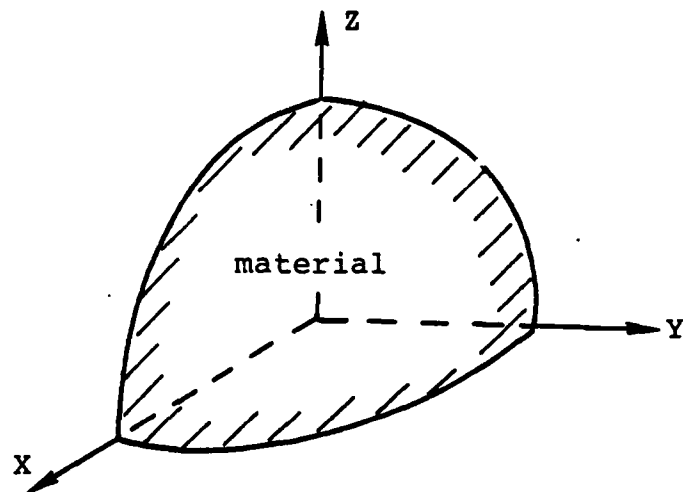


Detail around point M

Fig. 4 Crack in a laminated composite



(a) Exterior Problem



(b) Interior Problem

Fig. 5 Three dimensional corner formed  
by 3 mutually perpendicular planes.

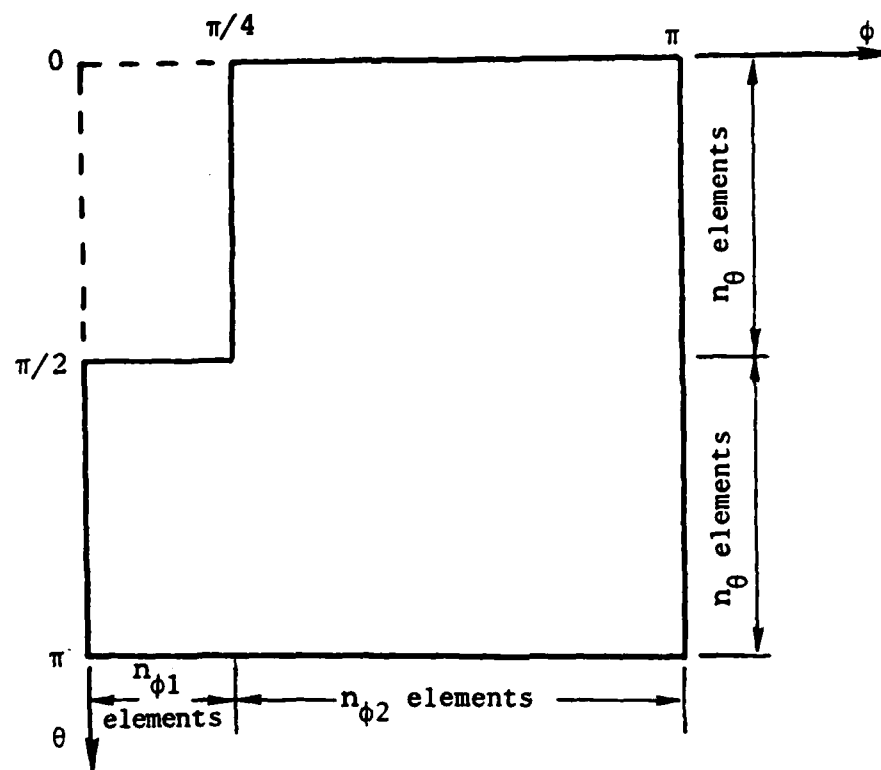


Fig. 6a Half of the domain of interest for 3-D corner exterior problem of Fig. 5a.

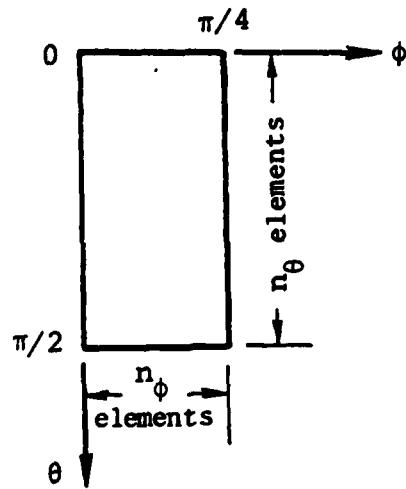


Fig. 6b Half of the domain of interest for 3-D corner interior problem of Fig. 5b.

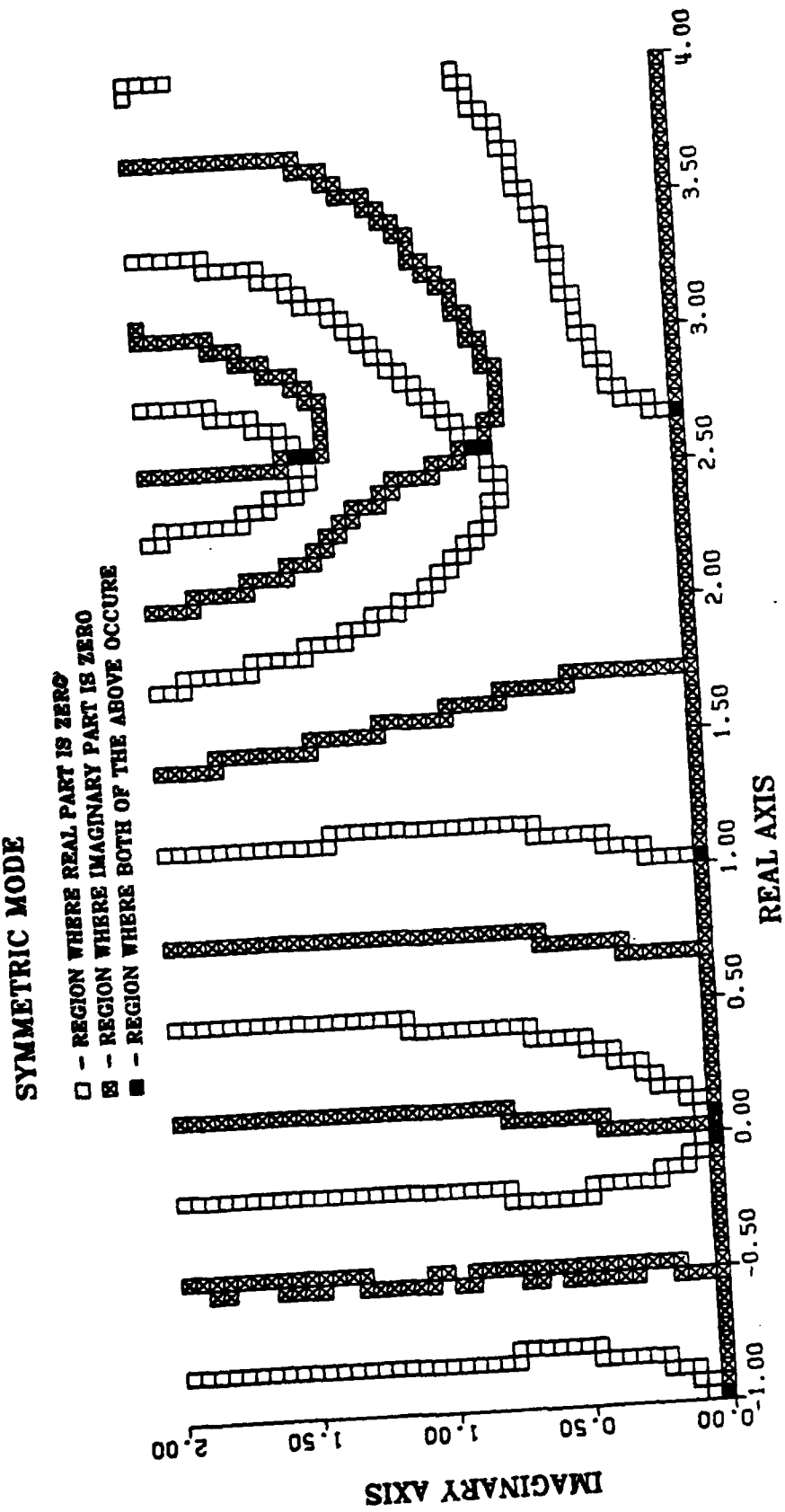
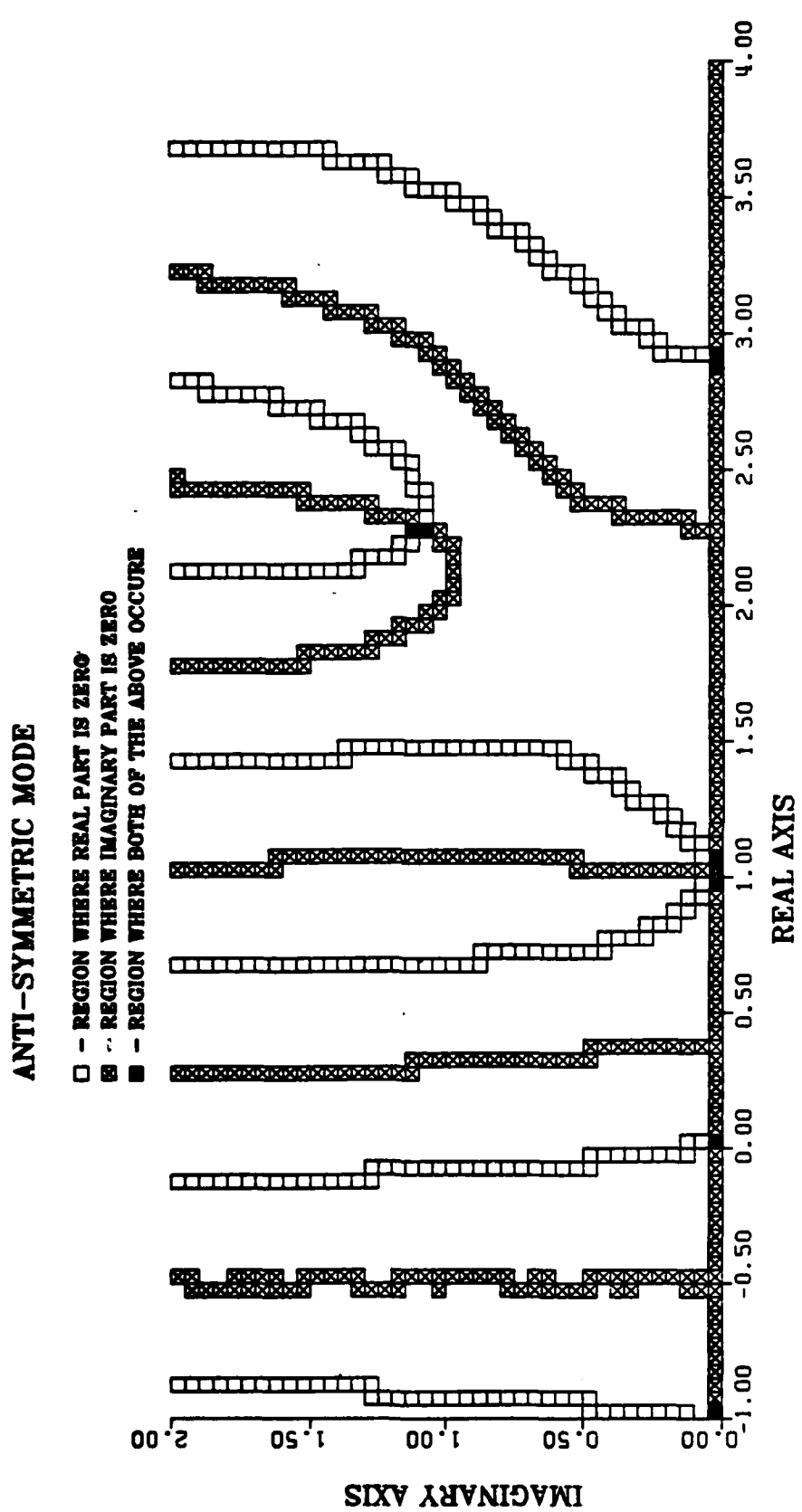


Figure 7 Plot of  $\operatorname{Re}(\|K\|) = 0$  and  $\operatorname{Im}(\|K\|) = 0$  on complex  $\lambda$  plane corresponding to 3-D corner interior problem, Fig. 5b, for composite-T material under symmetric mode of deformation.



**Figure 8** Plot of  $\operatorname{Re}(\|\lambda\|) = 0$  and  $\operatorname{Im}(\|\lambda\|) = 0$  on complex  $\lambda$  plane corresponding to 3-D corner interior problem, Fig. 5b, for composite - T material under anti-symmetric mode of deformation.

DISTRIBUTION LIST

No. of Copies

Office of Deputy Under Secretary of Defense for Research and Engineering (ET)	
ATTN: Mr. J. Persh, Staff Specialist for Materials and Structures (Room 3D1089)	1
The Pentagon Washington, DC 20301	
Office of Deputy Chief of Research Development and Acquisition	
ATTN: DAMA-CSS	1
The Pentagon Washington, DC 20301	
Commander	
U.S. Army Materiel Command	
ATTN: AMCLD, R. Vitali, Office of Laboratory Management	1
5001 Eisenhower Avenue	
Alexandria, VA 22333	
Director	
Ballistic Missile Defense Systems Command	
ATTN: BMDSC-TEN, N. J. Hurst	1
BMDSC-HE, J. Katechis	1
BMDSC-HNS, R. Buckelew	1
BMDSC-AOLB	1
P.O. Box 1500	
Huntsville, AL 35807	
Director	
Ballistic Missile Defense Advanced Technology Center	
ATTN: ATC-X, D. Russ	1
ATC-X, COL K. Kawano	1
ATC-M, D. Harmon	1
ATC-M, J. Papadopoulos	1
ATC-M, S. Brockway	1
P.O. Box 1500	
Huntsville, AL 35807-3801	
Director	
Defense Nuclear Agency	
ATTN: SPAS, MAJ D. K. Apo	1
SPLH, J. W. Somers	1
SPLH, Dr. B. Steverding	1
Washington, DC 20305-1000	

No. of Copies

Director	
Army Ballistic Research Laboratories	
ATTN: DRDAR-BLT, Dr. N. J. Huffington, Jr.	1
DRDAR-BLT, Dr. T. W. Wright	1
DRDAR-BLT, Dr. G. L. Moss	1
Aberdeen Proving Ground, MD 21005	
Commander	
Harry Diamond Laboratories	
ATTN: DRXDO-NP, Dr. F. Wimenitz	1
2800 Powder Mill Road	
Adelphi, MD 20783	
Commander	
Air Force Materials Laboratory	
Air Force Systems Command	
ATTN: LNC, Dr. D. Schmidt	1
Wright Patterson Air Force Base	
Dayton, OH 45433	
Commander	
BMO/ABRES Office	
ATTN: BMO/MNRT, COL R. Smith	1
Norton Air Force Base, CA 92409	
Commander	
Air Force Materials Laboratory	
ATTN: AFML/MBM, Dr. S. W. Tsai	1
Wright-Patterson Air Force Base	
Dayton, OH 45433	
Commander	
Naval Ordnance Systems Command	
ATTN: ORD-03331, Mr. M. Kinna	1
Washington, DC 20360	
Naval Postgraduate School	
ATTN: Code NC4(67WT),	
Professor E. M. Wu	1
Monterey, CA 93943	
Commander	
Naval Surface Weapons Center	
ATTN: C. Lyons	1
C. Rowe	1
Silver Springs, MD 20910	

	<u>No. of Copies</u>
Lawrence Livermore Laboratory ATTN: Dr. W. W. Feng P.O. Box 808 (L-342) Livermore, CA 94550	1
Sandia Laboratories ATTN: Dr. W. Alzheimer Dr. M. Forrestal Div. 1524 Dr. E. P. Chen P.O. Box 5800 Albuquerque, NM 87115	1 1 1
Aerospace Corporation ATTN: Dr. R. Cooper P.O. Box 92957 Los Angeles, CA 90009	1
AVCO Corporation Government Products Group ATTN: Dr. W. Reinecke P. Rolincik 201 Lowell Street Wilmington, MA 01997	1 1
ETA Corporation ATTN: D. L. Mykkanen P.O. Box 6625 Orange, CA 92667	1
Fiber Materials, Inc. ATTN: M. Subilia, Jr. L. Landers R. Burns Biddeford Industrial Park Biddeford, ME 04005	1 1 1
General Electric Company Advanced Materials Development Laboratory ATTN: K. Hall J. Brazel 3198 Chestnut Street Philadelphia, PA 19101	1 1
General Dynamics Corporation Convair Division ATTN: J. Hertz 5001 Kearny Villa Road San Diego, CA 92138	1

	<u>No. of Copies</u>
General Research Corporation ATTN: Dr. R. Wengler Dr. R. Parisse J. Green 5383 Hollister Avenue Santa Barbara, CA 93111	1 1 1
Kaman Sciences Corporation ATTN: Dr. D. C. Williams P.O. Box 7463 Colorado Springs, CO 80933	1
Ktech ATTN: Dr. D. Keller 911 Pennsylvania Avenue, N.E. Albuquerque, NM 87110	1
Lehigh University Institute of Fracture and Solid Mechanics ATTN: Dr. George C. Sih Bldg. 39, Packard Lab Bethlehem, PA 18015	1
Los Alamos National Laboratory ATTN: Dr. W. D. Birchler Mail Stop G787 Los Alamos, NM 87545	1
Martin Marietta Aerospace ATTN V. Hewitt Frank H. Koo P.O. Box 5837 Orlando, FL 32805	1
Massachusetts Institute of Technology Department of Aeronautics and Astronautics ATTN: Prof. T. H. H. Pian Cambridge, MA 02139	1
Pacifica Technology, Inc. ATTN: Dr. Ponsford P.O. Box 148 Del Mar, CA 92014	1
University of Illinois at Chicago Dept. of Civil Eng., Mech. & Metallurgy ATTN: Dr. R. L. Spilker Dr. T. C. T. Ting Box 4348, Chicago, IL 60680	1 1

	<u>No. of Copies</u>
Rohr Industries, Inc. ATTN: Dr. T. H. Tsiang MZ-19T P.O. Box 878 Chula Vista, CA 92012-0878	1
Radkowski Associates ATTN: Dr. P. Radkowski P.O. Box 5474 Riverside, CA 92507	1
Southwest Research Institute ATTN: A. Wenzel 8500 Culebra Road San Antonio, TX 78206	1
SPARTA Inc. ATTN: G. Wonacott 1055 Wall Street Suite 200 P.O. Box 1354 La Jolla, CA 92038	1
Terra Tek, Inc. ATTN: Dr. A. H. Jones 420 Wakara Way Salt Lake City, UT 84108	1
Defense Documentation Center Cameron Station, Bldg. 5 5010 Duke Station Alexandria, VA 22314	2
<b>Director</b> Army Materials and Mechanics Research Center ATTN: AMXMR-B, J. F. Dignam AMXMR-B, Dr. S. C. Chou AMXMR-B, L. R. Aronin AMXMR-B, Dr. D. P. Dandekar AMXMR-K AMXMR-PL Watertown, MA 02172	1 5 1 1 1 2

AB	Unclassified
	Unlimited Distribution
	<b>Key Words</b>
	Composite materials
	Stress singularity
	Finite Elements
	Variational principle
	Eigenfunctions
	Anisotropy
	3-D Analysis
Army Materials and Mechanics Research Center Watertown, Massachusetts 02172 <b>THREE-DIMENSIONAL STRESS SINGULARITIES IN ANISOTROPIC MATERIALS AND COMPOSITES</b> H. Somaraju and T. C. T. Ting Department of Civil Engineering, Mechanics and Materials University of Illinois at Chicago Chicago, Illinois 60607 Technical Report AFMC TR 85-26, August 1985, 61 pp. Title-Station, Contract AFMCR-31-1-73133 DIA Project: 60533500215 AFMC Code: 493000-21506 Final Report, March 1983 to August 1984	<p>A general numerical procedure is presented for determining the 3-dimensional stress singularities in anisotropic materials and composites. The geometry near the singular point can be represented by a conical wedge whose lateral surface is generated by straight lines passing through the wedge apex. The shape <math>S_1</math> of the cross section of the conical wedge at any constant radial distance defines the geometry of the 3-dimensional singular point in the material. If <math>S_1</math> consists of two regions each occupied by a different material, we have a 3-dimensional composite conical wedge. A finite element scheme based on variational principles is used to find the order of stress singularities at the wedge apex. The method can be applied to any shape of <math>S_1</math>. Several examples are presented. The method can be compared with the </p>

A general numerical procedure is presented for determining the 3-dimensional stress singularities in anisotropic materials and composites. The geometry near the singular point can be represented by a conical wedge whose lateral surface is generated by straight lines passing through the wedge apex. The shape  $S_1$  of the cross section of the conical wedge at any constant radial distance defines the geometry of the 3-dimensional singular point in the material. If  $S_1$  consists of two regions each occupied by a different material, we have a 3-dimensional composite conical wedge. A finite element scheme based on variational principles is used to find the order of stress singularities at the wedge apex. The method can be applied to any shape of  $S_1$ . Several examples are presented. For comparison with the existing numerical schemes for isotropic materials, the method is applied to special geometry and to isotropic materials. It is shown that the a mode higher order isoparametric elements employed here is very efficient in obtaining a fairly accurate result.

**Army Materials and Mechanics Research Center**  
Watertown, Massachusetts 02172  
**THREE-DIMENSIONAL STRESS SINGULARITIES**  
**IN ANISOTROPIC MATERIALS AND COMPOSITES**  
N. Senerman and T. C. T. Ting  
Department of Civil Engineering, Mechanics  
and Metallurgy,  
University of Illinois at Chicago  
Chicago, Illinois 60680  
Contract DAAG16-75-K-0133  
Technical Report AFML TR 85-24, August 1985, 61 pp.  
Tables, Contract DAAG16-75-K-0133  
Key Words  
Composite materials  
Stress singularity  
Finite Elements  
Variational principle  
Signfunctions  
Anisotropy  
S-0 Analysis

A general numerical procedure is presented for determining the 3-dimensional stress singularities in anisotropic materials and composites. The geometry near the singular point can be represented by a conical wedge whose lateral surface is generated by straight lines passing through the wedge apex. The shape  $S_1$  of the cross section of the conical wedge at any constant radial distance defines the geometry of the 3-dimensional singular point in the material. If  $S_1$  consists of two regions each occupied by a different material, we have a 3-dimensional composite conical wedge. A finite element scheme based on variational principles is used to find the order of stress singularities at the wedge apex. The method can be applied to any shape of  $S_1$ . Several examples are presented. For comparisons with the existing numerical schemes for isotropic materials, the method is applied to special geometry and to isotropic materials. It is shown that the 8 node higher order isoparametric elements employed here is very efficient in obtaining a fairly accurate result.

A general numerical procedure is presented for determining the 3-dimensional stress singularities in anisotropic materials and composites. The geometry near the singular point can be represented by a conical wedge whose lateral surface is generated by straight lines passing through the wedge apex. The shape  $S_1$  of the cross section of the conical wedge at any constant radial distance defines the geometry of the 3-dimensional singular point in the material. If  $S_1$  consists of two regions each occupied by a different material, we have a 3-dimensional composite conical wedge. A finite element scheme based on variational principles is used to find the order of stress singularities at the wedge apex. The method can be applied to any numerical shape of  $S_1$ . Several examples are presented. For comparisons with the existing numerical schemes for isotropic materials, the method is applied to special geometry and to isotropic materials. It is shown that the 6-node higher order isoparametric elements employed here are more effective than the 4-node quadrilateral elements.

AD Unclassified Unlimited Distribution

Key Words Composite materials Stress singularity Plastic Elements Variational principle Bifunctions Anisotropy 3-d Analysis

**Army Materials and Mechanics Research Center**  
Watertown, Massachusetts 02172

**THREE-DIMENSIONAL STRESS SINGULARITIES  
IN ANISOTROPIC MATERIALS AND COMPOSITES**

H. S. Siores and T. C. Ting  
Department of Civil Engineering, Mechanics  
and Metallurgy  
University of Illinois at Chicago  
Chicago, Illinois 60680

**Technical Report AFMRC TR 85-24 August 1985 01-22**

III-1-00005, Contract AFMRC-85-T-0139

D/A Project: #H263390010215  
AFMRC Code: 605000, 21506  
AFMRC Date: 10/10/85

A general numerical procedure is presented for determining the 3-dimensional stress singularities in anisotropic materials and composites. The geometry near the singular point can be represented by a conical wedge whose lateral surface is generated by straight lines passing through the wedge apex. The shape  $S_1$  of the cross section of the conical wedge at a given constant radial distance defines the geometry of the 3-dimensional singular point in the anisotropic material. If  $S_1$  consists of two regions such occupied by a different material, we have a 3-dimensional composite conical wedge. A finite element scheme based on variational principles is used to find the order of stress singularities at the wedge apex. The method can be applied to any shape of  $S_1$ . Several examples are presented. For comparisons with the existing numerical schemes for isotropic materials, the method is applied to special geometries reduced to isotropic materials. It is shown that the 6 mode higher order isoparametric elements are very efficient in obtaining a fairly accurate result.

**END**

**FILMED**

**12-85**

**DTIC**